RESPONSES OF ARRAYS OF ISOTROPIC ELEMENTS IN DETECTION AND TRACKING

Additive array found best for detection in a uniform noise field; split-beam multiplicative array best for bearing estimates of a single point target

L. K. Arndt • Research Report • 21 April 1967

U. S. NAVY ELECTRONICS LABORATORY, SAN DIEGO, CALIFORNIA

NEL / REPORT 1456

THE PROBLEM

Provide in a single reference the analytical expressions for the response of transducer arrays of standard form. Establish the most important factors in selecting a particular configuration for target detection and/or bearing estimation.

RESULTS

1. Analytical expressions of responses for linear, planar, cylindrical, and spherical arrays are given.

2. Additive arrays are "best" for detection of a point target in a uniform noise field.

3. Split-beam multiplicative arrays are "best" for bearing estimates of a single point target.

RECOMMENDATION

Use the analytical expressions of array response as a basis for computer programs used in predicting sonar performance.

ADMINISTRATIVE INFORMATION

Work was performed under S23-26, Task 8553 (NEL J80173). The report covers work from July 1966 to February 1967 and was approved for publication 21 April 1967.

REVERSE SIDE BLANK

CONTENTS

TABLES

ILLUSTRATIONS

ILLUSTRATIONS (Continued)

INTRODUCTION

In the continuing effort to improve the capabilities of sonar systems, the most common form of signal processing, and one of the most useful, has been by the use of directional transmitting and receiving transducer arrays. The array arrangement makes it possible to place greater power in the water and direct that power as desired. Directivity offers important advantages over omnidirectional systems. In the transmitting transducer, directivity provides a greater percent of the output energy in a desired direction (in the main beam) and thus provides more energy on target (if it is in the main beam) than would be provided by an omnidirectional transducer. In the receiving array, the directivity discriminates against any noise sources which are not in the main beam, and thus improves the signal-to-noise ratio. Considering the reciprocity of antenna systems, all transducer systems may be considered to operate as receivers.

In the study to be reported here, arrays of isotropic elements were used to provide directionality and so improve detection probability and parameter estimation -- the two major aspects of signal processing. For detection, the primary problem is to maximize the signal-to-noise ratio and at the same time meet other system requirements of size, frequency, bandwidth, scan time, time on target, etc. For parameter estimation (in this case direction of arrival of the wave front), improved sensitivity of the output to changes in the parameter is of importance, as well as signal-to-noise ratio.

The following section describes various arrays of isotropic elements to provide directionality. Subsequent sections are concerned with shading or weighting of the elements to reduce side-lobe level, and with some of the common forms of tracking systems used for bearing estimation.

ARRAYS OF ISOTROPIC ELEMENTS

Linear Arrays

The first array considered is a line of equally spaced isotropic elements (the response of an isotropic element is constant in all directions) as shown in figure 1. To obtain the far-field response due to a plane wave arriving at the array from an angle θ relative to the normal to the array, the output of each element is determined and then summed:

$$R(\theta) = \sum_k |R_k| \exp(i\psi_k)$$

where

$R(\theta)$	is the array response
R_k	is the amplitude response of the k^{th} element
ψ_k	is the phase at the k^{th} element

Since only the far-field response is being considered, the amplitude at each element is assumed equal and the response becomes

$$R(\theta) = A \sum_k \exp(i\psi_k)$$

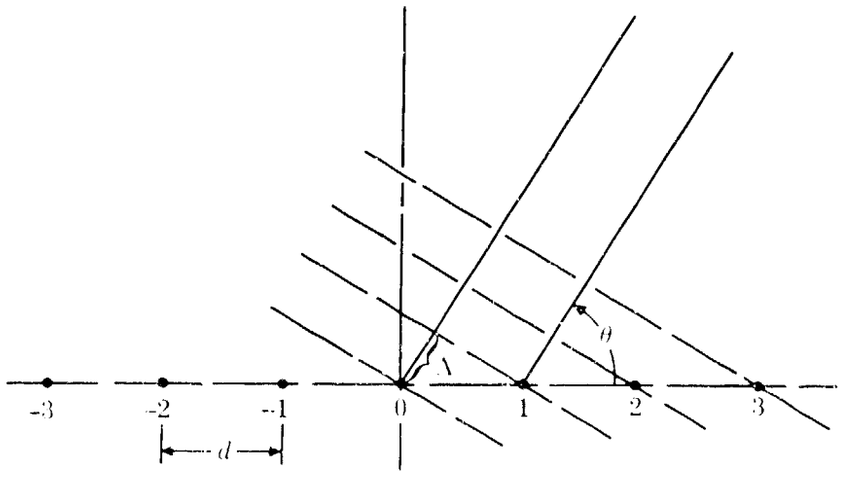

Figure 1. Geometry for uniform line array.

Referring again to figure 1, the phase at the k^{th} element relative to the center element is given by

$$\psi_k = \frac{k\Delta 2\pi}{\lambda} = \frac{2\pi k}{\lambda}\ d\cos\theta = kd_r\cos\theta$$

where d is the element spacing, $d_r = \frac{2\pi d}{\lambda}$,

and λ is the wavelength of the source. Thus

$$R(\theta) = A\sum_k \exp(ikd_r\cos\theta)$$

The sum from $-k_0$ to k_0 is of the form

$$\frac{R}{A} = \sum_{k=-k_0}^{k_0} \exp(ik\theta) = \exp(-ik\phi)$$

$$+\exp[-i(k_0-1)\phi + \cdots + 1 + \cdots + \exp[i(k_0-1)\phi] + \exp(ik_0\phi)$$

and

$$\exp(ik_0\phi)\cdot\frac{R}{A} = 1 + \exp(i\phi) + \exp(i2\phi) + \cdots + \exp(i2k_0\phi)$$

But

$$\frac{1-X^n}{1-X} = 1 + X + X^2 + \cdots + X^{n-1}$$

Therefore

$$\exp(ik_0\phi)\frac{R}{A} = \frac{1-\exp[i(2k_0+1)\phi]}{1-\exp(i\phi)}$$

and

$$\frac{R}{A} = \frac{\exp(-ik_0\phi)\exp[i(k_0+1)\phi]}{1-\exp(i\phi)} = \frac{\exp(-i\phi)\left(\frac{2k_0+1}{2}\right)\exp(i\phi)\left(\frac{2k_0+1}{2}\right)}{\exp\left(-i\frac{\phi}{2}\right)-\exp\left(i\frac{\phi}{2}\right)}$$

Since $2k_0 + 1 = n$, the total number of elements,

$$\frac{R}{A} = \frac{\exp\left(-\phi\frac{n}{2}\right)-\exp\left(i\phi\frac{n}{2}\right)}{\exp\left(-i\frac{\phi}{2}\right)-\exp\left(i\frac{\phi}{2}\right)} = \frac{\sin\frac{n\phi}{2}}{\sin\frac{\phi}{2}}$$

and

$$R(\theta) = \frac{A \sin \frac{nd_r}{2} \cos\theta}{\sin \frac{d_r}{2} \cos\theta}$$

If A is chosen to normalize the output to 1 when $\theta = 0$, then $A = 1/n$ and

$$R(\theta) = \frac{\sin \frac{nd_r}{2} \cos\theta}{n \sin \frac{d_r}{2} \cos\theta}$$

If a phase delay ϕ_0 is added to each element output such that the delay for the k^{th} element is $k\phi_0$ the response for the array will be given by

$$R(\theta) = \frac{\sin\left(\frac{nd_r}{2} \cos\theta - \frac{n\phi_0}{2}\right)}{n \sin\left(\frac{d_r}{2} \cos\theta - \frac{\phi_0}{2}\right)}$$

The proper phase delay between adjacent elements to steer the center of the main beam to θ_0 is $\phi_0 = d_r \cos\theta_0$ and the response is given by

$$R(\theta, \theta_0) = \frac{\sin \frac{nd_r}{2} (\cos\theta - \cos\theta_0)}{n \sin \frac{d_r}{2} (\cos\theta - \cos\theta_0)}$$

The response $R(\theta,\theta_0)$ is an amplitude pattern or directivity function or array factor. In determining directivity index and signal-to-noise power at the receiver, the power pattern is often of interest. The power pattern is proportional to the square of the magnitude of the directivity function:

$$P(\theta) = K |R(\theta)|^2$$

Planar Arrays

The directivity function of an array of isotropic elements is given by:

$$R = \sum_k R_k \exp(\phi_k)$$

where R_k is the amplitude of the k^{th} element

ϕ_k is the phase of the k^{th} element referenced to the origin.

The phase term is given by

$$\phi_k = \frac{2\pi}{\lambda} \Delta$$

where Δ is the difference in the distance from the source to the origin, D_o, and the distance from the source to the k^{th} element, D_k:

$$\Delta = D_o - D_k = \frac{D_o^2 - D_k^2}{D_o + D_k} = \frac{D_o^2 - D_k^2}{2D_o - \Delta}$$

If the source has coordinates x, y, z and the k^{th} element x_k, y_k, z_k then

$$x = D_o \cos \alpha_x \qquad x_k = \rho_k \cos \alpha_{xk}$$

$$y = D_o \cos \alpha_y \qquad y_k = \rho_k \cos \alpha_{yk}$$

$$z = D_o \cos \alpha_z \qquad z_k = \rho_k \cos \alpha_{zk}$$

with ρ_k the distance from the origin to the k^{th} element and $\alpha_x, \alpha_y, \alpha_z$ the angles shown in figure 2. Using these equations

$$\Delta = \frac{1}{2D_o - \Delta}\left[D_o^2 - (x - x_k)^2 - (y - y_k)^2 - (z - z_k)^2\right]$$

$$= \frac{1}{2D_o - \Delta}\left[2x\,x_k + 2y\,y_k + 2z\,z_k - (x_k^2 + y_k^2 + z_k^2)\right]$$

$$= \frac{2D_o \rho_k \cos \alpha_x \cos \alpha_{xk} + 2D_o \rho_k \cos \alpha_y \cos \alpha_{yk} + 2D_o \rho_k \cos \alpha_z \cos \alpha_{zk} - \rho_k^2}{2D_o - \Delta}$$

$$= \frac{\rho_k}{1 - \frac{\Delta}{2D_o}}\left[\cos \alpha_x \cos \alpha_{xk} + \cos \alpha_y \cos \alpha_{yk} + \cos \alpha_z \cos \alpha_{zk} - \frac{\rho_k}{2D_o}\right]$$

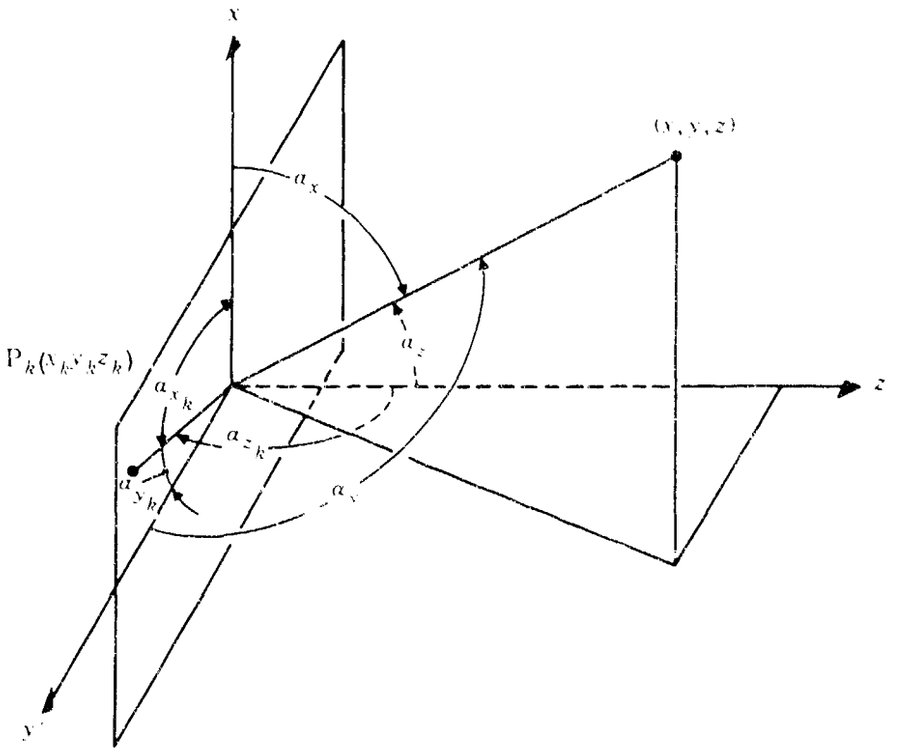

Figure 2. Geometry for planar array.

Since only the far field is of interest, $2D_o^2/\lambda \gg \Lambda$ and $2D_o^2/\lambda \gg \rho_k$. The phase of the k^{th} element is given by

$$\phi_k = \frac{2\pi\Lambda}{\lambda} - \frac{2\pi\rho_k}{\lambda}(\cos\alpha_x \cos\alpha_{xk} + \cos\alpha_y \cos\alpha_{yk} + \cos\alpha_z \cos\alpha_{zk})$$

$$\phi_k = \frac{2\pi}{\lambda}(x_k \cos\alpha_x + y_k \cos\alpha_y + z_k \cos\alpha_z)$$

For the special case of an equally spaced line array along the X-axis,

$$x_k = kd \qquad y_k = z_k = 0$$

and

$$\phi_k = \frac{2\pi kd}{\lambda}\cos\alpha_x$$

which is the same as obtained in the first section for a line array.

For the case of a rectangular array of equally spaced sources in the X-Y plane the phase of the mn^{th} element is

$$\phi_{mn} = \frac{2\pi}{\lambda}(md_x \cos \alpha_x + nd_y \cos \alpha_y) = \frac{2\pi mdx}{\lambda} \cos \alpha_x + \frac{2\pi ndy}{\lambda} \cos \alpha_y$$

$$\phi_{mn} = \phi_m + \phi_n$$

and the directivity function is given by

$$R(\alpha_x, \alpha_y) = \sum_{mn}^{MN} |R_{mn}| \exp(\phi_m) \cdot \exp(\phi_n)$$

If the amplitude, $|R_{mn}|$, is of the form

$$|R_{mn}| = |R_m| \cdot |R_n|$$

then the directivity function can be separated into a product of two factors

$$R(\alpha_x, \alpha_y) = \left[\sum_{m}^{M} |R_m| \exp(\phi_m)\right]\left[\sum_{n}^{N} |R_n| \exp(\phi_n)\right]$$

where each term is of the same form as for a linear array. Using the same reasoning as in the section on linear arrays, the case of $|R_m| = |R_n| = \frac{1}{MN}$ is given by

$$R(\alpha_x, \alpha_y) = \frac{\sin\left(\frac{M\pi dx}{\lambda} \cos \alpha_x\right)}{M \sin\left(\frac{\pi dx}{\lambda} \cos \alpha_x\right)} \cdot \frac{\sin\left(\frac{N\pi dy}{\lambda} \cos \alpha_y\right)}{N \sin\left(\frac{\pi dy}{\lambda} \cos \alpha_y\right)}$$

Thus

$$R(\alpha_x, \alpha_y) = R(\alpha_x, \pi/2) \cdot R(\pi/2, \alpha_y)$$

and the response is specified by the product of the response in the Y-Z plane and the response in the Y-Z plane. To use this separation of variables it is important to use the proper coordinate system. As an example, choose the θ, ϕ system shown in figure 3 and transform the response:

$$\cos \alpha_x = \sin \phi$$

$$\cos \alpha_y = \cos \phi \cos \theta$$

$$R(\theta, \phi) = \frac{\sin\left(\frac{M\pi d_x}{\lambda} \sin \phi\right)}{M \sin\left(\frac{\pi d_x}{\lambda} \sin \phi\right)} \cdot \frac{\sin\left(\frac{N\pi d_y}{\lambda} \cos \phi \cos \theta\right)}{N \sin\left(\frac{\pi d_y}{\lambda} \cos \phi \cos \theta\right)}$$

which is no longer a product of two functions each of which is a function of a single variable.

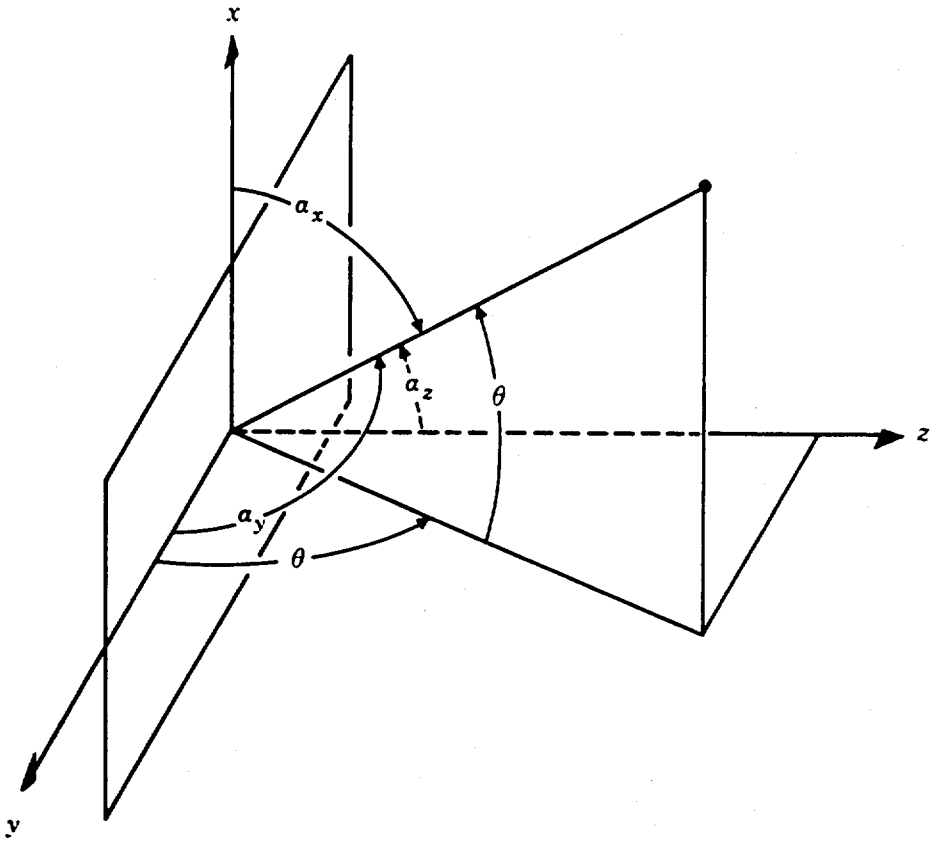

Figure 3. Geometry for azimuth-elevation coordinate system.

Introducing a phase shift between elements to steer the main beam to a direction $\cos \alpha_{xs}$, $\cos \alpha_{ys}$ and writing the response in terms of the differences of the direction cosines results in the following:

$$R(\tau_x, \tau_y) = \frac{\sin\left(\frac{Md_r}{2}\tau_x\right)}{M \sin\left(\frac{d_r}{2}\tau_x\right)} \cdot \frac{\sin\left(\frac{Nd_r}{2}\tau_y\right)}{N \sin\left(\frac{d_r}{2}\tau_y\right)}$$

where

$$\tau_x = \cos\alpha_x - \cos\alpha_{xs}$$

$$\tau_y = \cos\alpha_y - \cos\alpha_{ys}$$

$$d_r = \frac{2\pi dx}{\lambda} = \frac{2\pi dy}{\lambda}$$

For elements which are closely spaced in terms of wavelengths, the sine terms in the denominator may be approximated by their argument and the response is given by

$$R = \frac{\sin X}{X} \cdot \frac{\sin Y}{Y}$$

$$X = \frac{Md_r}{2}\tau_x = \frac{\pi Md}{\lambda_0}\tau_x$$

$$Y = \frac{Nd_r}{2}\tau_y = \frac{\pi Nd}{\lambda_0}\tau_y$$

Figure 4 is a plot of these equations near the main beam. Note that for a square array ($M=N$) the main beam is circular in cross section at the half-power points, and it is found to be elliptical for $M \neq N$. As R approaches the first null,

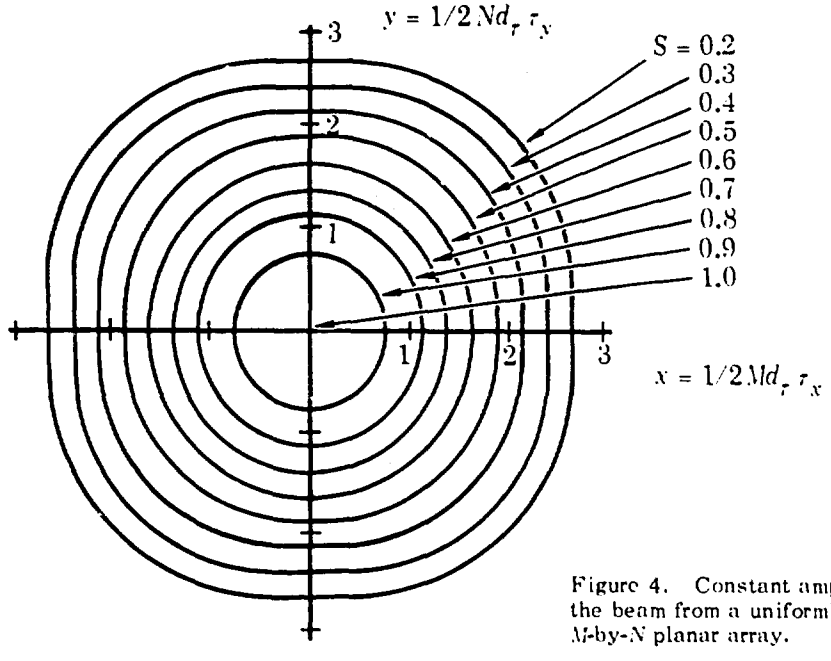

Figure 4. Constant amplitude plots of the beam from a uniformly illuminated M-by-N planar array.

a broadening of the beam along the diagonal is noted. The half-power beam width of a uniformly illuminated square array is given in τ-space as

$$2\,\Delta\tau = \frac{C_0}{A/\lambda}$$

where

$$C_0 = 0.888$$

$$A = Nd \text{ (length of the aperture)}$$

Other coefficients are applicable for other types of aperture illumination. In general, the main beam broadens and the side-lobe level is reduced as the illumination function is tapered. Further discussion of tapering or shading the illumination will appear later in the report.

The main advantage in using the τ-space is that the beam shape is not a function of the scan position of the beam when plotted in τ-space. The beam maximum is scanned by introducing a phase difference ψ_x and ψ_y between elements in the array. The direction cosines corresponding to the phase shifts are

$$\cos\alpha_{xs} = \frac{\psi_x}{d_r} \qquad \cos\alpha_{ys} = \frac{\psi_y}{d_r}$$

If a complex T-plane is defined by

$$T = \cos\alpha_x + i\cos\alpha_y$$

and

$$T_s = \cos\alpha_{xs} + i\cos\alpha_{ys}$$

then

$$T_s = \frac{\psi_x}{d_r} + i\frac{\psi_y}{d_r} \quad \frac{\psi}{d_r}$$

and

$$\psi = \psi_x + i\psi_y$$

The complex τ-plane now becomes

$$\tau = \tau_x + i\tau_y = T - T_s$$

The array response, which is a function of the complex variable τ, is invariant in the T-plane. Scanning the beam by introducing the complex phase delay $\psi = \psi_x + i\,\psi_y$ simply translates the pattern in space so that the pattern center moves to $T_s = \frac{\psi}{d}$. (See fig. 5.) If the phase delay is chosen such that $|T|>1$ the half-power contour moves outside the unit circle and becomes imaginary (i.e., unobservable).

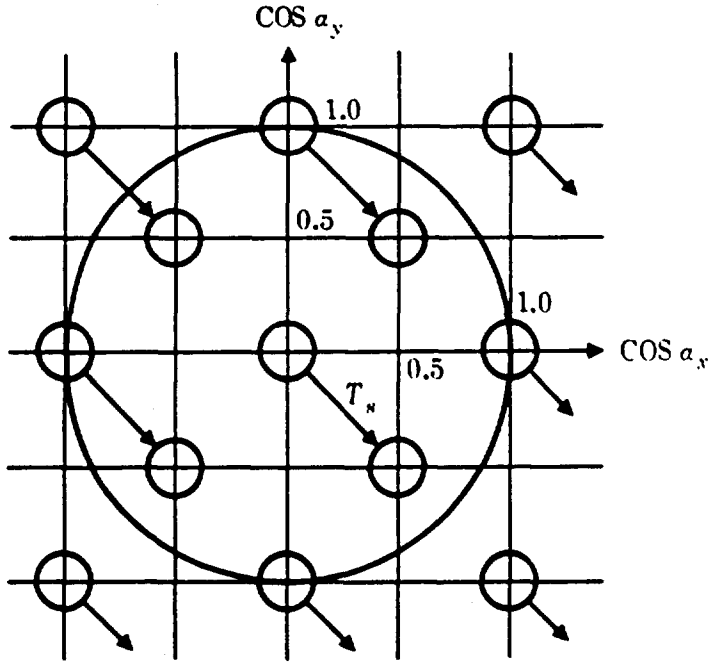

Figure 5. Scanning in the complex T plane with one wavelength element spacing.

The effects of scanning the main beam may now be considered in the T-plane with only a translation of the pattern being considered. Figure 5 shows the main beam and the secondary maxima of a square array of isotropic elements. The secondary maxima are spaced $\tau_{x0} = \tau_{y0} = \frac{\lambda_0}{d}$ apart and there are an infinite number of them. It must be remembered that only those contained within the unit circle are real. The larger the element space the closer the spacing of the secondary maxima and hence the greater number contained in the unit circle. If the elements are spaced one wavelength apart, the main beam and four end-fired secondary beams are visible and any scanning from broadside will move the end-fired beams within the unit circle. Closer spacing of the elements can suppress the secondary beams. For example, with $d = \frac{2\lambda_0}{3}$ no secondary maxima occur if $T_s < 1.2$ (fig. 6). Further suppression of secondary maxima is possible when using nonisotropic sources with low gain in the direction of the expected secondary maxima.

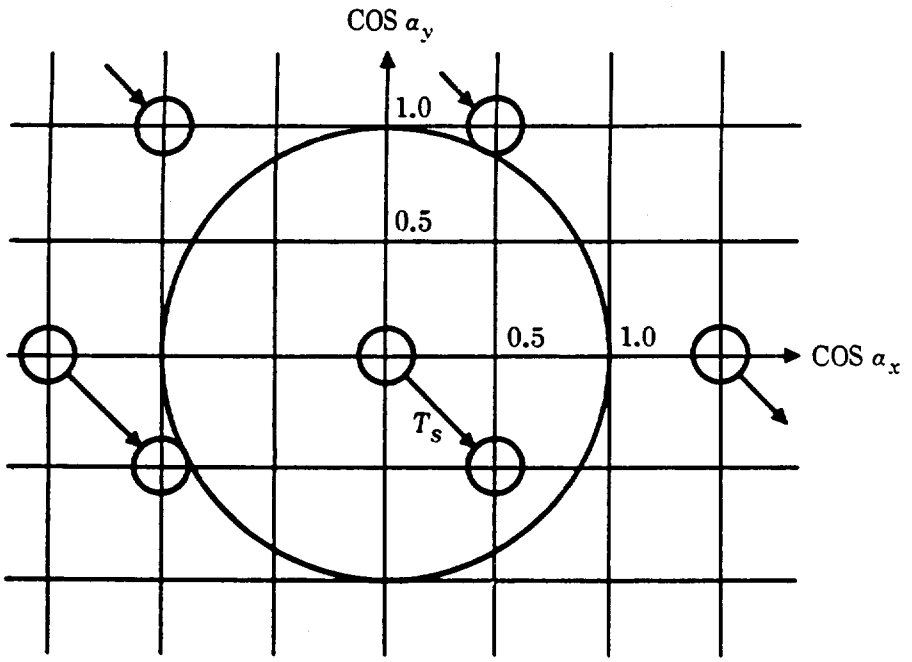

Figure 6. Secondary maxima of a scanned array with two-thirds wavelength element spacing.

The value of using the T-plane or direction cosine space when examining the effects of scanning the main beam of the array has been shown. However, to permit a physical interpretation, a transformation to a spherical coordinate system is necessary. The proper transformation is found by expressing the complex direction cosine, T, in polar coordinates:

$$T = \cos\alpha_x + i\cos\alpha_y = \sin\theta\cos\phi + i\sin\theta\sin\phi$$

$$T = \sin\theta(\cos\phi + i\sin\phi) = \sin\theta\exp(i\phi)$$

Hence, the desired transformation is the projection of the unit circle in the T-plane onto a unit sphere (fig. 7). By limiting the values of θ to $0 \leq \theta \leq \frac{\pi}{2}$ only the positive hemisphere is of interest. In the case of a rectangular array ($M \neq N$), the transformation is the same but the main and secondary maxima will be approximately elliptical in cross section rather than circular as discussed earlier.

Referring to figure 7, as the main beam is scanned away from the broadside position, the beam width changes. The reference beam width at broadside is

$$B_o = 2\sin^{-1}(\Delta r)$$

where

$$\Delta r = \frac{C_b\lambda_o}{2A}$$

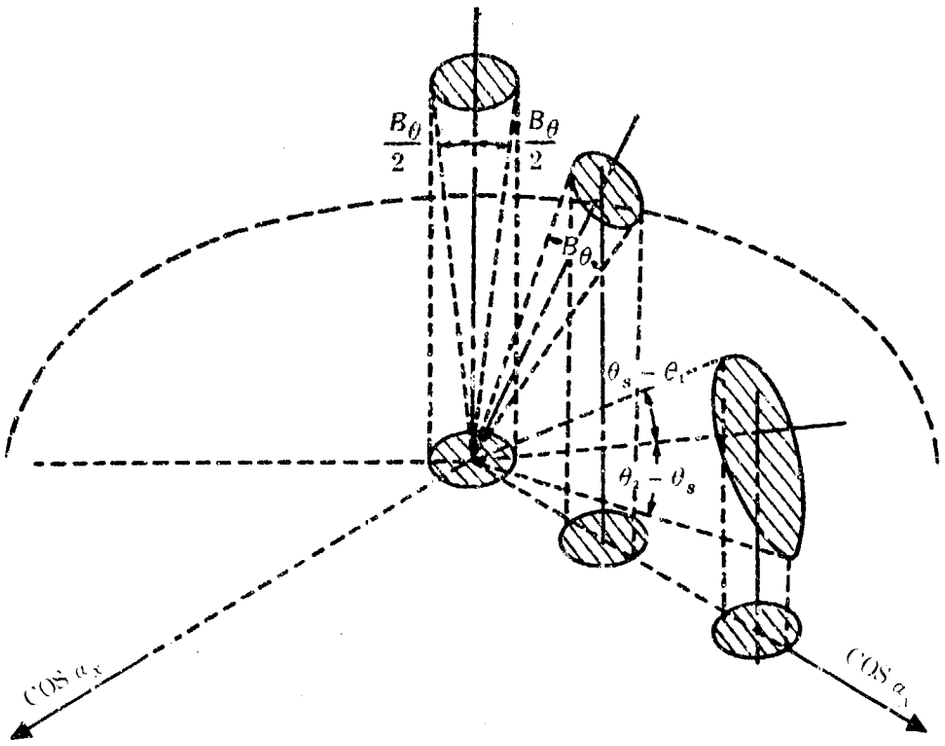

Figure 7. Beam width and eccentricity of the scanned beam.

As the beam is scanned, the beam width in the ϕ direction remains constant, while the beam width in the θ direction is obtained by

$$2\,\Delta z = T_2 - T_1 = \sin\theta_2 - \sin\theta_1$$

$$B_\theta = \theta_2 - \theta_1 = 2\sin^{-1}\frac{\Delta z}{\cos^{1/2}(\theta_2 - \theta_1)}$$

If the scan angle θ_s is less than $\pi/4$ and the beam width is small, then B_ϕ and B_θ can be approximated by

$$B_\phi \cong 2\,\Delta z$$

$$B_\theta = \frac{2\,\Delta z}{\cos^{1/2}(\theta_2 - \theta_1)} \cong \frac{B_\phi}{\cos\theta_s}$$

Thus, as the beam is scanned away from the normal, it broadens in the θ direction and the half-power contours for a square array change from circular to elliptical.

Because of the change in the beam shape, its maximum point is not centered between the half-power points. A beam eccentricity can be defined by

$$2e = \frac{(\theta_2 - \theta_s) - (\theta_s - \theta_1)}{(\theta_2 - \theta_s) + (\theta_s - \theta_1)}$$

Using the above equations as they apply to the half beams $\theta_2 - \theta_s$ and $\theta_s - \theta_1$ yields

$$2e = \tan 1/4\ (\theta_1 + \theta_2 + 2\theta_s)\ \tan 1/4\ (\theta_2 - \theta_1)$$

Approximating $\theta_1 + \theta_2 \simeq 2\ \theta_s$ and $\tan 1/4\ (\theta_2 - \theta_1) \simeq \frac{B_\theta}{4}$

yields

$$e \simeq \frac{B_\theta}{8} \tan \theta_s$$

The difference between the beam maximum and the center of the half-power contour, $\frac{\theta_1 + \theta_2}{2}$, is then

$$\Delta\theta = \frac{B_\theta^2}{8} \tan \theta_s$$

Thus, for narrow beams (i.e., B_θ small) the eccentricity may be neglected. Figure 8 is a plot of the pointing error vs scanning angle as a function of the broadside beam width.

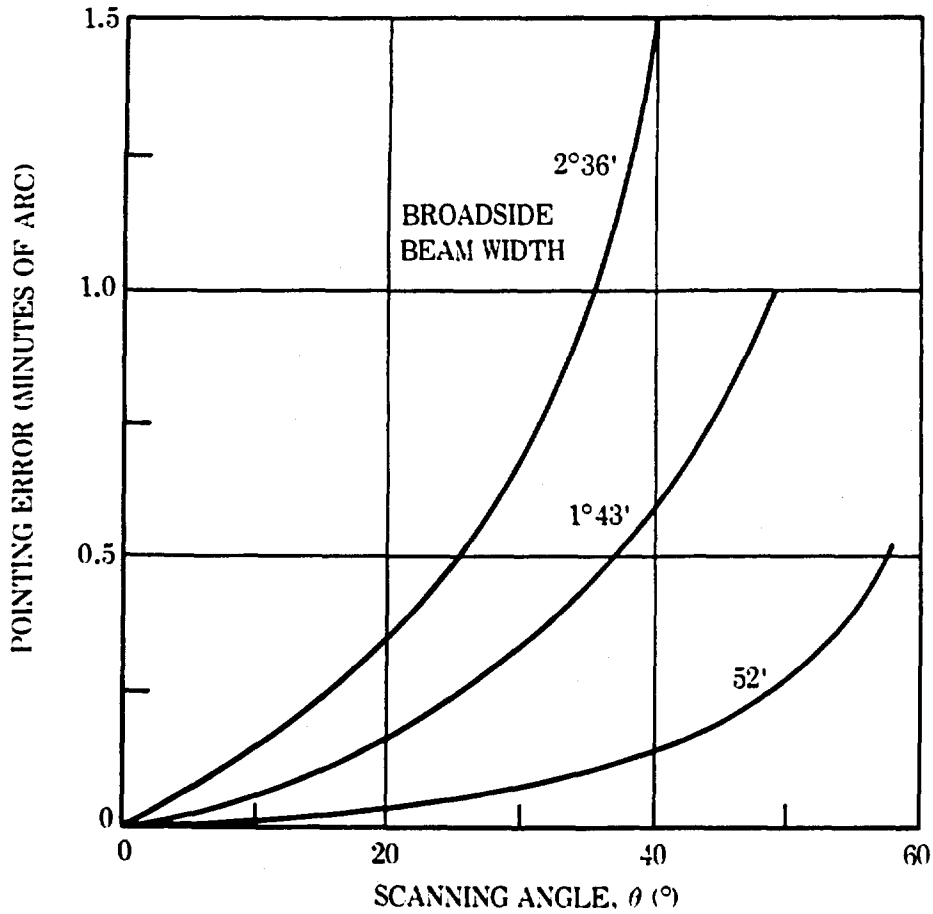

Figure 8. Pointing error vs scan angle as a function of the broadside beam width.

Nonuniform Illumination

The principles which have been developed will be applied to tapered illumination. The side-lobe level of a uniformly illuminated array is 13.2 dB below the main-beam intensity. To achieve lower side-lobe levels, tapering of the illumination across the array or weighting the output of each element is used. Many types of illumination tapers have been proposed for giving various relationships between gain, beam width, and side-lobe level. The choice of illumination taper will depend upon the relative emphasis placed on these three parameters.

The uniform distribution gives the 13.2-dB side-lobe level, theoretically the highest array gain for a uniform phase distribution and moderate beam width.

A second important illumination taper is shown as the Dolph-Chebyshev distribution. Using Chebyshev polynomials, Dolph has synthesized an illumination distribution giving uniform side lobes of any desired amplitude.[1] It was shown by Dolph that this distribution gives the narrowest beam width for any specified side-

[1]Superscript numbers identify references listed at end of report.

lobe level and conversely gives the lowest side-lobe level for a given beam width. In this respect, it is optimum. The distribution, being specified by polynomials, is given at discrete intervals only and is, therefore, ideally applicable only to arrays. The distribution is characterized by current peaks in the end elements which become inconveniently high for very long arrays with very low side lobes. For this reason, the Dolph-Chebyshev distribution is usually used only with arrays of moderate length.

Van der Maas[2] adapted the Dolph-Chebyshev distribution to a continuous aperture by allowing the number of elements to approach infinity. In the limit the far-field distribution approaches the function

$$F(U, A) = \cos \pi (U^2 - A^2)^{1/2}$$

where

$$U = \frac{Nd}{\lambda_0} \cos \alpha - \cos \alpha_s$$

and

$$\eta = \cosh \pi A \text{ is the side-lobe ratio}$$

This radiation pattern is physically unrealizable because of the requirement for infinite current peaks at the edges of the aperature.

Taylor[3] has modified Van der Maas's distribution, giving slightly greater beam width and higher gain for the same lobe level. The far-field pattern for a line array is given by[4]

$$F(U, A, \bar{\eta}) = \frac{\eta [\Gamma(\bar{\eta})]^2}{\Gamma(\bar{\eta} + U)\Gamma(\bar{\eta} - U)} \prod_{\eta=1}^{\bar{\eta}-1} 1 - \frac{U^2}{\sigma^2 [A^2 + (\eta - 1/2)^2]}$$

where

$$\sigma = \frac{\bar{\eta}}{[A^2 + (\bar{\eta} - 1/2)^2]^{1/2}}$$

The constant η is arbitrary but if it is set equal to cosh πA then $F(U, A, \bar{\eta})$ may be quite closely approximated in the region $|\frac{U}{\sigma}| < A$ by the function

$$F(U, A) = \cos \pi \left[A^2 - \left(\frac{U}{\sigma}\right)^2 \right]^{1/2}$$

Using this approximation, the beam width of the modified Taylor distribution is greater than that of the Dolph-Chebyshev limit by the factor σ. Figure 9 is a plot

of the beam widths as a function of the highest side-lobe level for a uniform illumination, the Dolph-Chebyshev limit, and the Taylor modified distribution, with $\bar{\eta}$ = 2, 4, 6, and 8. Note that the Dolph-Chebyshev limit has the narrowest beam width of any distribution at the same side-lobe level.

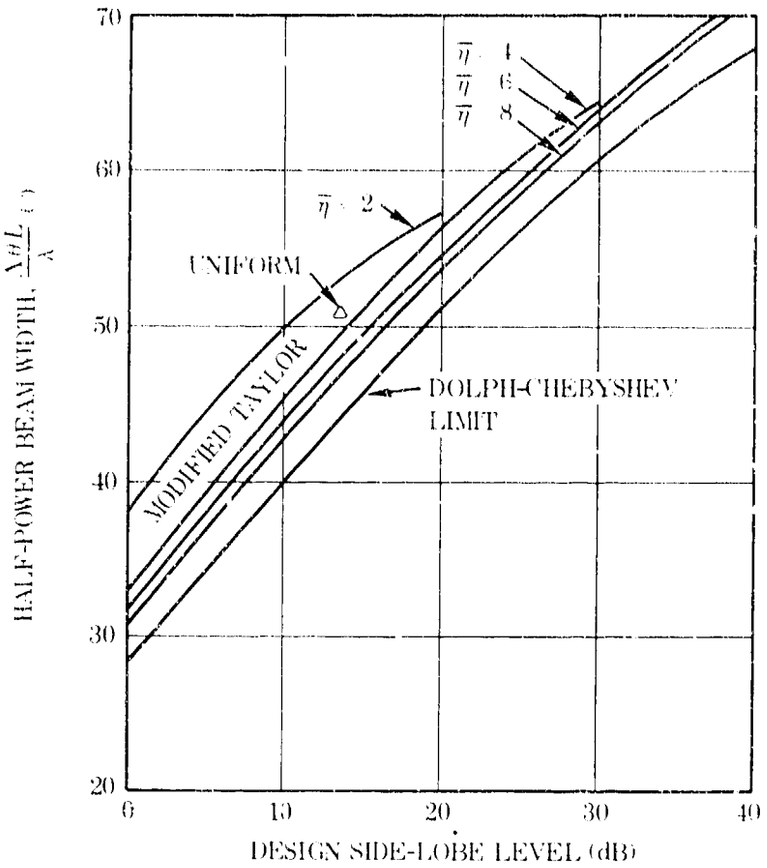

Figure 9. Normalized beam width as a function of design side-lobe level for a number of distributions.

The field pattern of the Taylor distribution has $(\bar{\eta} - 1)$ side lobes of almost equal amplitude adjacent to the main beam, followed by a region of monotonic decreasing side lobes. The power in the far-out sidelobes is reduced, returning it to the main beam and thus increasing the gain over that of the "ideal" Dolph-Chebyshev distribution. Figure 10A gives the plots of the gain for a Dolph-Chebyshev limited distribution as a function of the array length for several side-lobe levels. Figures 10B and 10C give the same information for the Taylor distributions with the number of uniform side lobes equal to half the total number and to a quarter of the total number. It is seen that these two distributions have the same gains for very low side-lobe levels but the gain deteriorates most rapidly for the Dolph-Chebyshev limit as the antenna size is increased and the side-lobe level is raised.

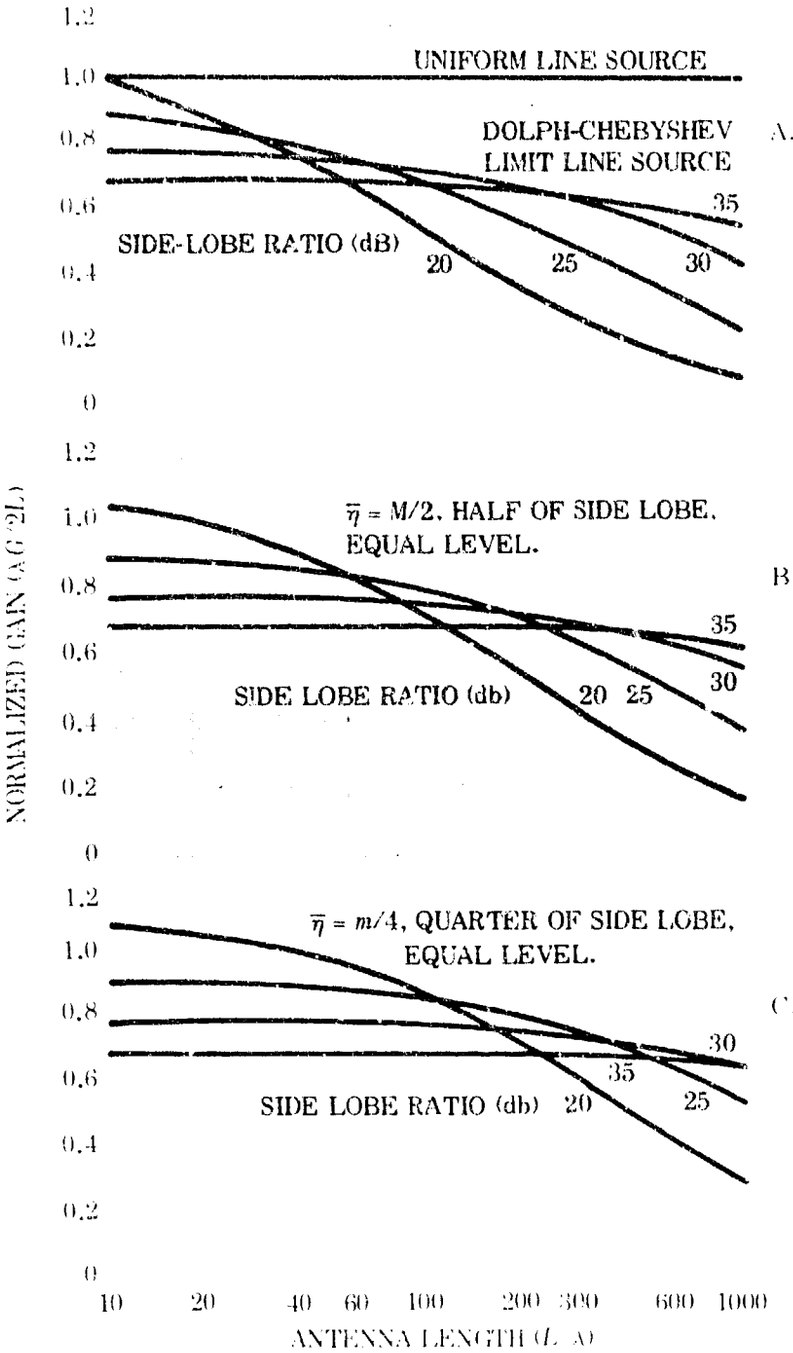

A. NORMALIZED GAIN VS LENGTH FOR UNIFORM AND DOLPH-CHEBYSHEV LIMIT SPACE FACTORS.

B. NORMALIZED GAIN VS LENGTH FOR TAYLOR MODIFIED SPACE FACTOR.

C. NORMALIZED GAIN VS LENGTH FOR TAYLOR MODIFIED SPACE FACTOR.

Figure 10. Normalized gain as a function of array size and design side-lobe level for three distributions.

A number of other illumination tapers are frequently used when moderate side lobes are required and the primary requirement is convenience and ease of calculation. A number of these, such as "truncated gaussian" and "cosine squared on a pedestal," give excellent results with side lobes approximately 25 dB down. A comparison of the change in beam width, pointing error, and gain will now be made for a 34 λ linear array at scan angles of 30 to 55 degrees, with uniform illumination versus a modified Taylor distribution. A 34 λ linear array of isotropic elements has a broadside half-power beam width of[5]

$$\theta_\eta = \frac{0.888}{L/\lambda_0} = 0.0261 \text{ radian} = 1.496 \text{ degrees}$$

The gain at broadside is[6]

$$G_\eta = \frac{2L}{\lambda_0} = 68 = 18.32 \text{ dB}$$

and the first side lobes are 13.2 dB below the main beam. When scanned to 30 degrees from the normal, the half-power beam width is increased to[5]

$$\theta_{30} = \frac{\theta_\eta}{\cos \frac{1}{2}(\theta_2 + \theta_1)}$$

where

$$\sin \theta_1 = \sin 30 - \sin \frac{\theta_\eta}{2}$$

$$\sin \theta_2 = \sin 30 + \sin \frac{\theta_\eta}{2}$$

Therefore

$$\theta_1 = 0.49372 \text{ radian}$$

$$\theta_2 = 0.55398 \text{ radian}$$

$$\theta_{30} = 0.0301427 \text{ radian} = 1.727 \text{ degrees}$$

The point of maximum gain is displaced from halfway between the half-power points by

$$\Delta\theta_{30} = \frac{\theta_{30}^2}{8} \tan 30^\circ = 6.55769 \times 10^{-5} \text{ radians}$$

$$= 13.526 \text{ seconds}$$

and the gain is reduced by the "projected area"

$$G_{30} = G_\eta \cos \theta_s = 58.89 \simeq 17.70 \text{ dB}$$

or a loss of 0.62 dB compared with the gain at broadside. All calculations are based on isotropic elements. The directivity of the elements may be taken into account as outlined by Von Aulock.[5]

With a scan angle of 55 degrees from the normal, the half-power beam width is

$$\theta_{55} = \frac{\theta_\eta}{\cos \tfrac{1}{2} (\theta_2 + \theta_1)}$$

$$\theta_1 = 0.93764 \text{ radian}$$

$$\theta_2 = 0.98311 \text{ radian}$$

$$\theta_{55} = 0.0455 \text{ radian} = 2.607 \text{ degrees}$$

The maximum gain is displaced by

$$\Delta\theta_{55} = \frac{\theta_{55}^2}{8} \tan 55$$

$$\Delta\theta_{55} = 3.6959 \times 10^{-4} \text{ radians} = 0.021176 \text{ degree}$$

$$= 76.73 \text{ seconds}$$

The gain at the can angle of 55 degrees is

$$G_{55} = G_\eta \cos \theta_s = 39.00 \text{ or } 15.91 \text{ dB}$$

for a 2.41-dB reduction compared to broadside.

The modified Taylor distribution chosen for comparison has a side-lobe level of 30-dB (power) below the main beam and $\bar{\eta} = 6$. The ratio of the beam width of the main lobe compared to that of the Dolph-Chebyshev is given by

$$\sigma = \frac{\bar{\eta}}{[A^2 + (\bar{\eta} - \tfrac{1}{2})^2]^{\frac{1}{2}}}$$

where

$\eta = \cosh \pi A$ is the voltage side-lobe ratio

Thus.

$$\sigma = \frac{6}{[1.74229 + (6 - \frac{1}{2})^2]^{\frac{1}{2}}} = \frac{6}{5.656} = 1.0608$$

and the main lobe is approximately 6 percent wider than a Dolph-Chebyshev (DC) with the 30-dB side-lobe level which is given by

$$\theta_{DC} = 60.6 \frac{\lambda_0}{L} \text{ (degrees)}$$

compared to that of a uniform illumination given by

$$\theta = 50.9 \frac{\lambda_0}{L} \text{ (degrees)}$$

The ratio of the main beam of a modified Taylor distribution with side lobes 30 dB down to a uniform illumination with side lobes 13.2 dB down is

$$\rho = \sigma \cdot \frac{60.6}{50.9} = \sigma\ 1.19056 = 1.262946$$

given a beam width at broad side for a 34 λ linear array of

$$\theta_T = \sigma\ 60.6 \frac{\lambda_0}{L} \text{ (-30 dB side lobes)}$$

$$= 1.890 \text{ degrees} = 0.03299 \text{ radian}$$

The gain of the modified Taylor distribution relative to the uniform is given by[7]

$$\frac{\lambda G}{2 L} \simeq \frac{2 \eta^2}{1.93 A \eta^2 + 2 (\bar{\eta} - 1)}$$

for

$$\eta^2 = 10^3$$

$$A = 1.32$$

$$\bar{\eta} = 6$$

$$\frac{\lambda G}{2 L} = 0.782 \text{ or } -1.06 \text{ dB}$$

or

$$G = 53.18 \text{ or } 17.26$$

At a scan angle of 30 degrees, the half-power beam width has increased to

$$\theta_{30} = 2.18 \text{ degrees} = 0.038048 \text{ radian}$$

and the gain decreased to

$$G_{30} \simeq 46.05 \text{ or } 16.63 \text{ dB}$$

The displacement of the maximum gain point from midway between the half-power points is

$$\Delta\theta_{30} = \frac{\theta_{30}^2}{8} \tan 30 \text{ (radians)}$$

$$= \frac{0.38038)^2}{8} (0.5774)$$

$$= 1.0448 \times 10^{-4} \text{ radians} = 21.55 \text{ seconds}$$

With a phase delay between elements to give a 55-degree scan angle, the half-power beam width is increased to

$$\theta_1 = 0.9318$$

$$\theta_2 = 0.9893$$

$$\theta_{55} = 0.57519 \text{ radian} = 3.295 \text{ degrees}$$

The gain at 55-degree scan angle is reduced to

$$G_{55} = 53.18 \cos 55 = 30.5 \text{ or } 14.84 \text{ dB}$$

The displacement of the maximum gain point is

$$\Delta\theta_{55} = \frac{(0.057519)^2}{8} \times 1.4282$$

$$= 5.906 \times 10^{-4} \text{ radians} = 121.83 \text{ seconds}$$

Table 1 summarizes the above results for a linear array of isotropic elements 34 wavelengths long.

TABLE 1. SIDE-LOBE LEVEL FOR UNIFORM AND MODIFIED TAYLOR ILLUMINATION

	Scan Angle from Broadside (°)		
	0	30	55
Uniform Illumination:			
Side-lobe level (dB down from main beam)	13.2	13.2	13.2
Half-power beam width (degrees)	1.496	1.727	2.607
(radians)	0.0261	0.03014	0.0455
Gain (ratio)	68.0	58.9	39.0
(dB)	18.32	17.70	15.91
Displacement of beam center (radians)	- -	6.558×10^{-5}	36.959×10^{-5}
(arc sec.)	- -	13.53	76.23
Modified Taylor Illumination ($\bar{\eta} = 6$):			
Side-lobe level (dB down from main beam)	30.0	30.0	30.0
Half-power beam width (degrees)	1.890	2.18	3.296
(radians)	0.03299	0.03805	0.057519
Gain (ratio)	53.18	46.05	30.5
(dB)	17.26	16.63	14.84
Displacement of beam center (radians)	- -	10.448×10^{-5}	59.06×10^{-5}
(arc sec.)	- -	21.55	121.83

Cylindrical Arrays

Referring to figure 11, the response or directivity function for a cylindrical array is given by

$$R = \sum_{s,\,t} |R_{st}| \exp 2i\phi_{st}$$

where t is an index for the stave of the element and s is an index for the element location on the stave with the (0,0) element being located on the Z axis.

The phase, ϕ_{st}, referenced to the origin is given by

$$\phi_{st} = \frac{2\pi}{\lambda} (x_{st} \cos\alpha_x + y_{st} \cos\alpha_y + z_{st} \cos\alpha_z)$$

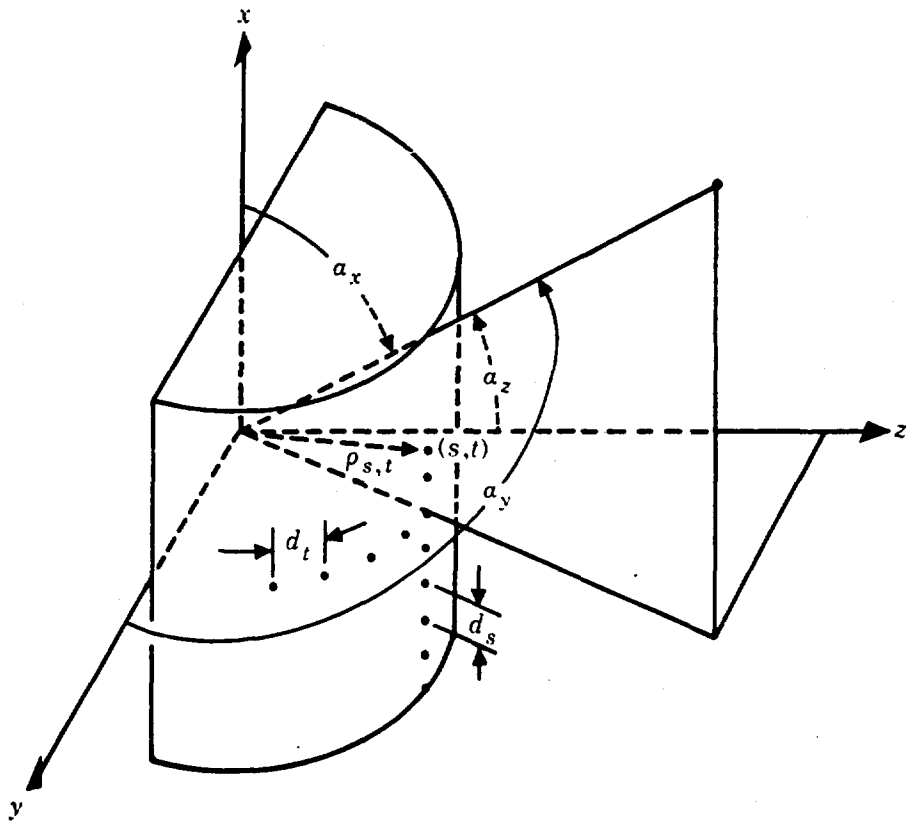

Figure 11. Geometry for cylindrical array.

The coordinates for the s, t element are given by

$$x = sd_s$$

$$y = r \sin\left(\frac{td_t}{r}\right)$$

$$z = r \cos\left(\frac{td_t}{r}\right)$$

where

d_s is the element separation in the x direction

d_t is the arc distance between staves

r is the radius of the cylinder

and

$$\phi_{st} = \frac{2\pi r}{\lambda}\left[\frac{sd_s}{r}\cos\alpha_x + \sin\left(\frac{td_t}{r}\right)\cos\alpha_y + \cos\left(\frac{td_t}{r}\right)\cos\alpha_z\right]$$

If phase compensation is added to give a maximum response in the $(\alpha x_s, \alpha y_s, \alpha z_s)$ direction the phase of the (s,t) element is given by

$$\phi = \frac{2\pi r}{\lambda}\left[\frac{sd_s}{r}(\cos\alpha_x - \cos\alpha_{xs}) + \sin\left(\frac{td_t}{r}\right)(\cos\alpha_y - \cos\alpha_{ys}) + \cos\left(\frac{td_t}{r}\right)(\cos\alpha_z - \cos\alpha_{zs})\right]$$

For the special case of compensation for a plane wave along the Z-axis the phase is

$$\cos\alpha_x = 0 \qquad \cos\alpha_y = 0 \qquad \cos\alpha_z = 1$$

$$\phi = \frac{2\pi r}{\lambda}\left[\frac{sd_s}{r}\cos\alpha_x + \sin\left(\frac{td_t}{r}\right)\cos\alpha_y + \cos\left(\frac{td_t}{r}\right)(\cos\alpha_z - 1)\right]$$

The first term in the equation for phase with general compensation is the only term which depends on the index s and it is in the same form as the response for a linear array. Thus if the amplitude term is <u>not</u> a function of s the response may be written in the form

$$R = \sum_s \exp(i\phi_s) \cdot \sum_t |R_t| \exp(i\phi_t)$$

$$|R_t| = n\,|R_{st}|$$

$$\phi_s = \frac{2\pi}{\lambda} sd_s\,(\cos\alpha_x - \cos\alpha_{xs})$$

$$\phi_t = \frac{2\pi r}{\lambda}\left[\sin\frac{td_t}{r}(\cos\alpha_y - \cos\alpha_{ys}) + \cos\frac{td_t}{r}(\cos\alpha_z - \cos\alpha_{zs})\right]$$

and

$$R_s = \sum_s \exp(i\phi_s) = \frac{\sin\left[\frac{n\pi d_s}{\lambda}(\cos\alpha_x - \cos\alpha_{xs})\right]}{n\sin\left[\frac{\pi d_s}{\lambda}(\cos_x - \cos_{xs})\right]}$$

where n is the number of elements in a stave. The response of the cylindrical array with no shading along the axis of the cylinder may be viewed as the product of the response due to a line array and an arc array. The response for the arc of a circle is

$$R = \sum_t R_t \exp(i\phi_t)$$

$$\phi_t = \frac{2\pi r}{\lambda}\left[\sin\frac{td_t}{r}(\cos\alpha_x - \cos\alpha_{xs}) + \cos\frac{td_t}{r}(\cos\alpha_z - \cos\alpha_{zs})\right]$$

For the special case where the array is compensated for a plane wave arriving in the x-z plane but with a tilt angle of ϕ_c the response is given by

$$R = R_t \cdot R_s$$

$$R_s = \frac{\sin\left[\frac{n\pi d_s}{\lambda}(\cos\alpha_x - \sin\phi_c)\right]}{n\sin\left[\frac{\pi d_s}{\lambda}(\cos\alpha_x - \sin\phi_c)\right]}$$

$$R_t = \sum_t R_t \exp(i\phi_t)$$

$$\phi_t = \left[\frac{2\pi r}{\lambda}\sin\left(\frac{td_t}{r}\right)\cdot\cos\alpha_y + \cos\left(\frac{td_t}{r}\right)(\cos\alpha_z - \cos\beta_c)\right]$$

Since compensation in azimuth is normally done by selecting the stave in the desired direction as the center of the arc the above case is a very general one.

Figure 12 is an example of a pattern calculated for the case of

$$\beta_c = 0$$

$$\alpha_x = \pi/2$$

α_z in 5° steps

$$\frac{2\pi r}{\lambda} = 24$$

16 staves separated by 7.5° around the cylinder;

8 omnidirectional elements per stave ($s_0 = 1$)

$$R_t = \cos^2\frac{(2t+1)d_t}{2r}$$

The plot is of $10\log R(\alpha,0)^2 - 10\log R(0,0)^2$. Note the relatively large response to the rear of the array. This may be reduced by using elements which are themselves directional, having very low response in the rear hemisphere.

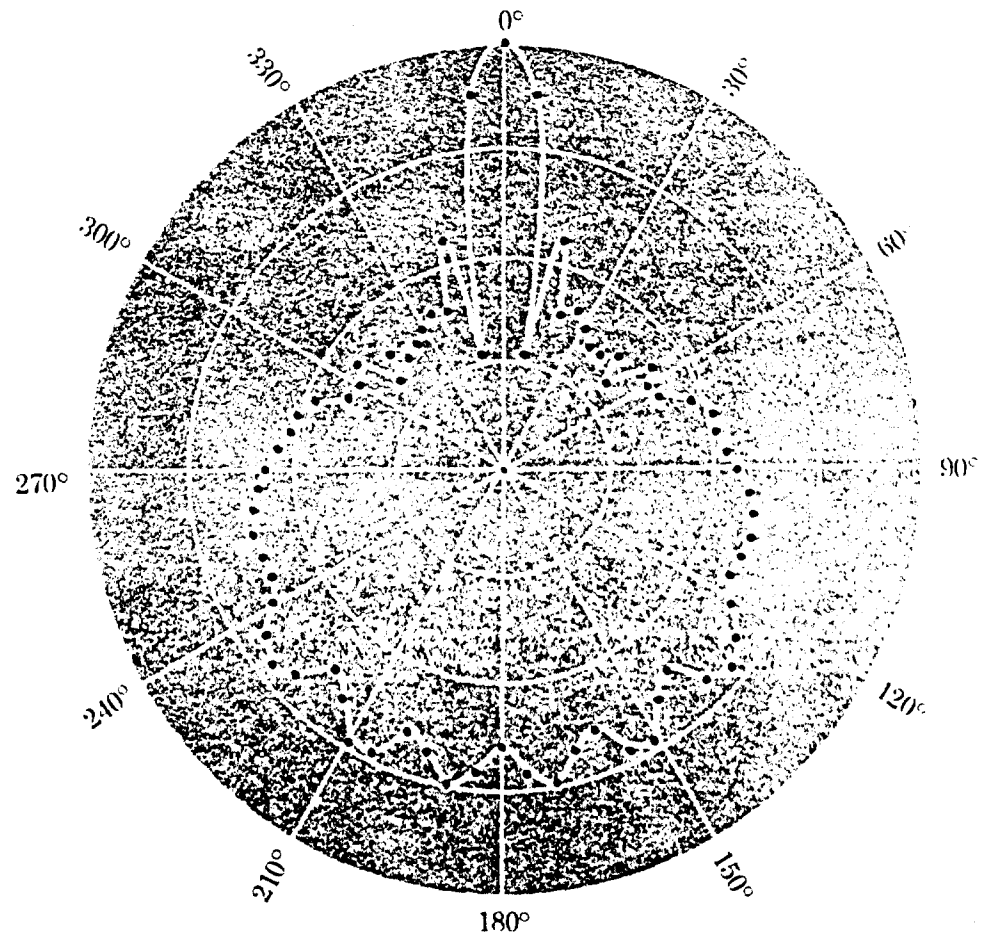

Figure 12. Response in Y-Z plane for cylindrical array.

Spherical Arrays

The equations for the response of an array of point sources is easily extended to the case where the sources are arranged on the surface of a transparent sphere with diameter ρ. The general equation for the phase of the k^{th} element with direction cosines $\alpha_{xk}, \alpha_{yk}, \alpha_{zk}$ and distance from the origin ρ_k is given by

$$\phi_k = \frac{2\pi\rho_k}{\lambda}(\cos\alpha_{xk}\cos\alpha_x + \cos\alpha_{yk}\cos\alpha_y + \cos\alpha_{zk}\cos\alpha_z)$$

where the reference point is the origin and the incoming plane wave has direction cosines $\alpha_x, \alpha_y, \alpha_z$ (see fig. 13). If the array is compensated to give a maximum response in the $(\alpha_{xs}, \alpha_{ys}, \alpha_{zs})$ direction the resulting phase for the k^{th} element is given by:

$$\phi_{ks} = \frac{2\pi\rho}{\lambda}\left[\cos\alpha_{xk}\left(\cos\alpha_x - \cos\alpha_{xs}\right) + \cos\alpha_{yk}\left(\cos\alpha_y - \cos\alpha_{ys}\right)\right.$$

$$\left. + \cos\alpha_{zk}\left(\cos\alpha_z - \cos\alpha_{zs}\right)\right]$$

where the subscript was dropped from ρ since the distance from the origin is the same for each element of the spherical array. Because of the large number of possible arrangements of the elements on the sphere and the fact that most of those arrangements used in practice do not result in any great simplification of the equations, they shall be left in the general form as given. The resulting response is given by

$$R = \sum_k |R_k| \exp(i\phi_k)$$

The amplitude term is used to account for the sphere not being transparent, the directional response of the individual elements, and any shading function which is incorporated.

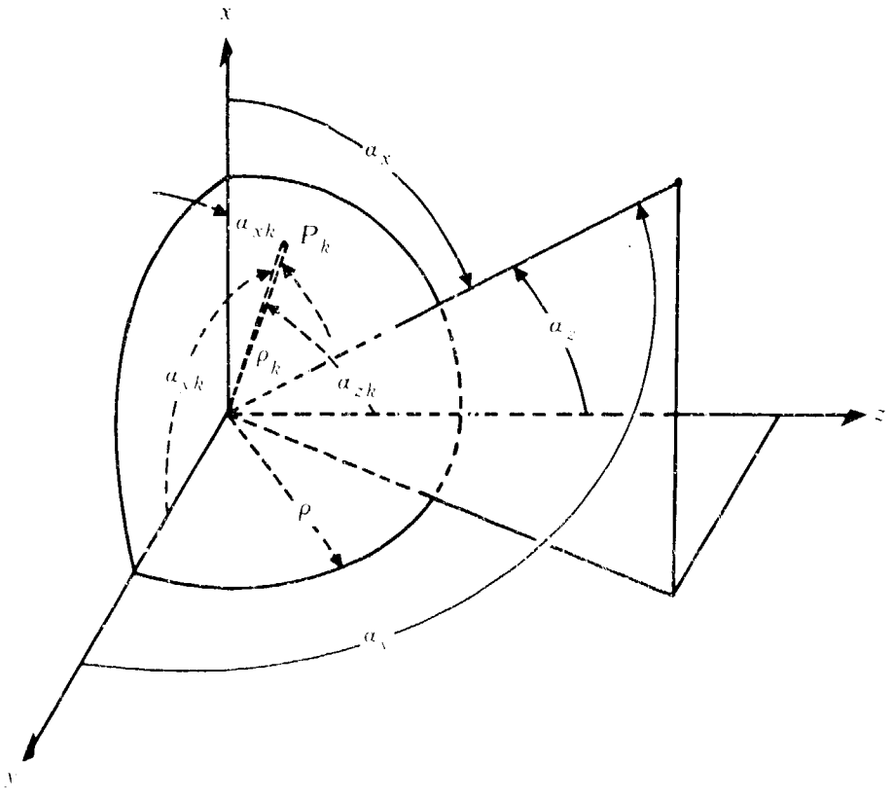

Figure 13. Geometry for spherical array.

ANGULAR TRACKING SYSTEMS

The characteristics of several sonar tracking techniques were studied to determine the most suitable for an ASW system employing a planar transducer array. The choice of the "best" technique from those available was approached by comparing their performance trade-offs in applications to an ASW planar array with their characteristics in applications to an array of equally spaced elements.

The characteristics of the various tracking techniques were summarized after a study of the literature.* The following section presents comparative discussions of the techniques studied, and summaries of their major features.

The main basis for comparison in the study was an additive system which forms a narrow beam by the summation in phase of all the outputs of the array elements. Of particular interest are sum and difference systems such as those used in monopulse tracking and the "split-beam" multiplicative arrays often used in passive systems.

Of special concern in the study were the directional pattern, noise factor, and tracking sensitivity. The directional pattern defines the one-way array gain when evaluated along the boresight, and the main lobe size as measured between the first set of nulls. In general, each system will provide an even-order pattern with a maximum at boresight for detection and an odd-order pattern with a null at boresight for use in tracking the detected target.

One other form of the phase for the k^{th} element may be useful. If the difference of direction cosines are replaced by the τ_x, τ_y, and τ_z terms and the location of the k^{th} elements is left in rectangular coordinates, then ϕ_k is given by

$$\phi_k = \frac{2\pi}{\lambda}\left(x_k\tau_x + y_k\tau_y + z_k\tau_z\right)$$

$$R = \sum_k |R_k| \left[\exp\left(\frac{2\pi x_k \tau_x}{\lambda}\right)\right]\left[\exp\left(\frac{2\pi y_k \tau_y}{\lambda}\right)\right]\left[\exp\left(\frac{2\pi z_k \tau_z}{\lambda}\right)\right]$$

In the next section the effect of the array configuration on angular tracking of the target will be examined.

---

* Specific references are cited in the discussion; other pertinent literature is also included in the References section, page 61.

Additive Linear Array

The general configuration of an additive line array, which will be used as the basis of comparison between systems, is shown in figure 14. The overall length of the array is D with n elements spaced d apart. With an input signal of $A \cos \omega_0 t$, the summing of the n equally weighted transducers outputs gives the following[8]

$$\Sigma = \frac{\sin\left(n \frac{\pi d}{\lambda} \sin\theta\right)}{\sin\left(\frac{\pi d}{\lambda} \sin\theta\right)} A \cos \omega_0 t$$

The symbol Σ shall be used for the output of each beam-forming channel and Λ for the output of the nulling channels even though they are most often associated with the sum and difference channels of monopulse systems. The context will make clear the system being considered.

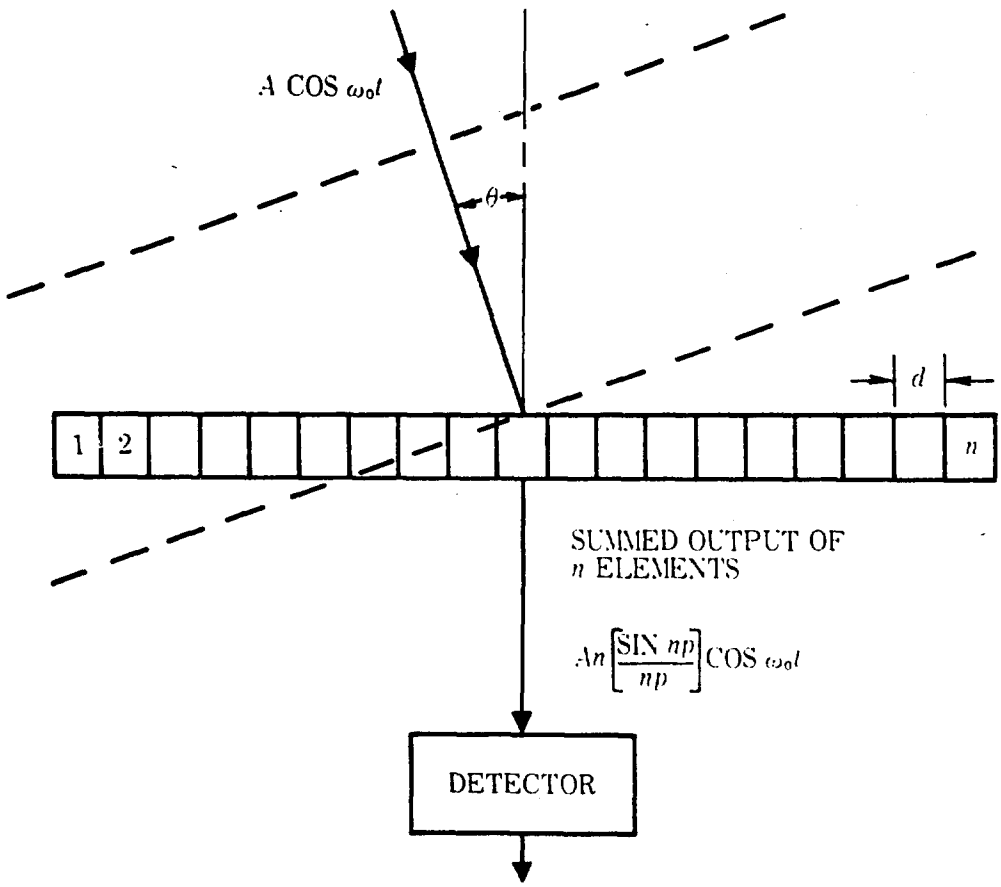

Figure 14. Block diagram of additive line array.

Using the variable $p = \frac{\pi d}{\lambda} \sin\theta$ and noting that for closely spaced elements the sine function in the denominator may be replaced by its argument gives

$$\Sigma = An\left(\frac{\sin np}{np}\right)\cos\omega_0 t$$

The introduction of time delays between the elements and summing network provides for steering the main beam. Since the only change in the expression given is that p is replaced by p' where $p' = \frac{\pi d}{\lambda}(\sin\theta - \sin\theta_a)$ and θ_a is the steering angle introduced, the effects of beam steering will not be included.

When a beam-forming system is used to estimate the angular location of the target as well as to detect the target, the best estimate of target bearing is the boresight of the beam with a standard deviation of approximately the half-power beam width (half angle). Thus very little can be said about the bearing except that the target is contained within the beam (assuming that the side lobes have been reduced to a negligible level).

In radar and some types of sonar systems, a moving antenna lobe is used to improve the angular accuracy. Many types of lobe-switching and beam-scanning tracking systems have been developed, all of which have the common disadvantage of requiring several samples of target data to give an estimate of the angle of arrival. This is undesirable in systems where the target returns undergo fluctuations between sample points. In the case of sonar these fluctuations are due to target motion between samples, changes in the propagation path, platform motion, etc.

Systems which obtain the information necessary to make an estimate of the angle of arrival on the basis of a single sample or pulse are classed as simultaneous-lobing, or monopulse, systems.

Figure 15 shows one way of processing the outputs of the linear array to obtain a better estimate of the target bearing. The array is divided into two equal sub-arrays where outputs are summed and differenced. The sum channel will provide a beam at boresight for use in detection and the difference channel will give a null at boresight to be used in tracking.

The outputs of each of the sub-arrays are given by

$$E_1 = \frac{An}{2}\left(\frac{\sin\frac{np}{2}}{\frac{np}{2}}\right)\cos\left(\omega_0 t - \frac{\phi}{2}\right)$$

$$E_2 = \frac{An}{2}\left(\frac{\sin\frac{np}{2}}{\frac{np}{2}}\right)\cos\left(\omega_0 t + \frac{\phi}{2}\right)$$

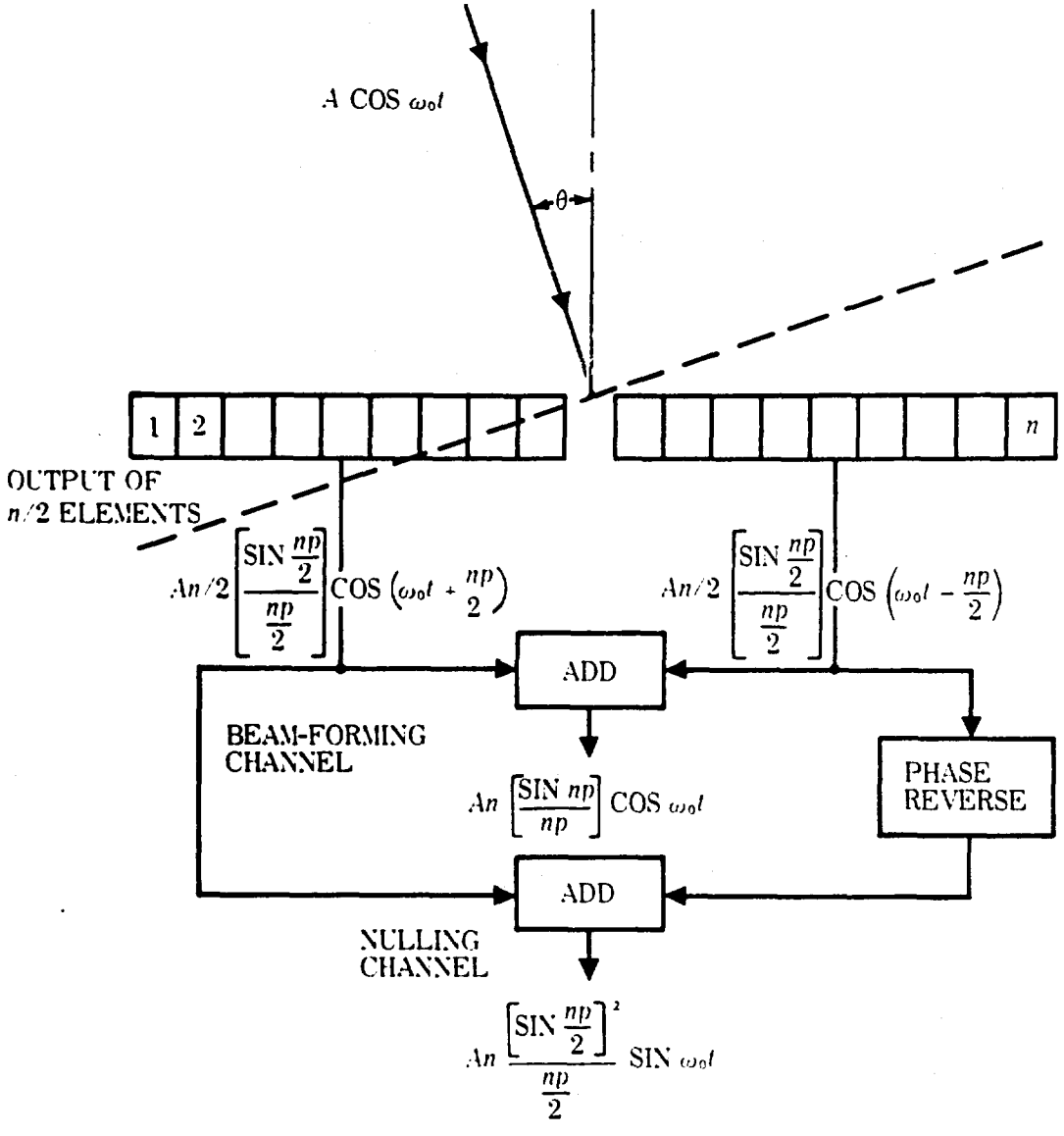

Figure 15. Split-beam additive array.

where

$$\phi = \frac{n\pi d}{\lambda} \sin\theta = np$$

The sum of the two sub-arrays is

$$\Sigma = E_1 + E_2 = \frac{An}{2}\left(\frac{\sin\frac{np}{2}}{\frac{np}{2}}\right)\left[\cos\left(\omega_0 t - \frac{np}{2}\right) + \cos\left(\omega_0 t + \frac{np}{2}\right)\right]$$

$$= \frac{An}{2}\left(\frac{\sin\frac{np}{2}}{\frac{np}{2}}\right)\left[2\left(\cos\omega_0 t\right)\left(\cos\frac{np}{2}\right)\right]$$

$$= \frac{A}{p}\left[2\left(\sin\frac{np}{2}\right)\left(\cos\frac{np}{2}\right)\right]\cos\omega_0 t$$

$$\Sigma = An\,\frac{\sin np}{np}\cos\omega_0 t$$

which, as would be expected, is the response previously stated for the summed output for the full array. The difference channel output is given by

$$\Delta = E_1 - E_2 = \frac{An}{2}\left(\frac{\sin\frac{np}{2}}{\frac{np}{2}}\right)\left[\cos\left(\omega_0 t - \frac{np}{2}\right) - \cos\left(\omega_0 t + \frac{np}{2}\right)\right]$$

$$= \frac{An}{2}\left(\frac{\sin\frac{np}{2}}{\frac{np}{2}}\right)\left(2\sin\omega_0 t\sin\frac{np}{2}\right)$$

$$= An\,\frac{\left(\sin\frac{np}{2}\right)^2}{\frac{np}{2}}\sin\omega_0 t$$

The difference function, Δ, is an odd function with a null at $p = 0$ which makes it a useful function for tracking a target in angle. Since the accuracy with which the null point can be determined is limited by the noise present in the difference channel and is proportional to the slope of the function at the null, a measure of the system sensitivity is the ratio of the slope of the direction pattern at $p = 0$ to the rms noise level in the difference channel for some normalized input signal. The slope of the split-beam additive system difference channel envelope is

$$\Delta' = \lim_{p \to 0} \frac{d\Delta}{dp} = \lim_{p \to 0} 2A \frac{pn\left(\sin\frac{np}{2}\right)\left(\cos\frac{np}{2}\right) - \left(\sin\frac{np}{2}\right)^2}{p^2}$$

$$= 2A \lim_{p \to 0} \frac{\frac{n^2p}{2}\left(\cos\frac{np}{2}\right)^2 - \frac{n^2p}{2}\left(\sin\frac{np}{2}\right)^2}{2p}$$

$$\Delta' = \frac{n^2 A}{2}$$

Thus the sum channel may be used to detect the signal and the difference channel used to track the target within the beam width of the sum channel. If it is desired to estimate the position of the target relative to the boresight rather than maintain the target at the null, it is necessary to eliminate the dependence on the signal amplitude in the difference channel. It was shown that for the additive linear array the difference signal and the slope of the difference signal with respect to angle of arrival are both functions of the input signal amplitude. To eliminate this dependence on signal amplitude the sum-channel signal may be used to control an AGC loop in the difference channel. A system of this type is known as a phase-sensing monopulse system.

Monopulse Tracking Systems

The two basic types of monopulse systems are classed as amplitude sensing and phase sensing. They are distinguished by the type of antenna system used to produce the sum and difference signals. After the sum and difference signals are produced, their processing may be the same in either system. A summary of each type will be given here; a detailed development and analysis of each may be found in references 9, 10, and 11.

Two of the requirements of a true monopulse system are that an odd function of the angle of arrival be formed and that this function be normalized so that it is not a function of the absolute value of the received signal. By using only the ratio of the signal amplitudes the system is made insensitive to target-strength fluctuations due to variations in the propagation media or target scintillation.

In the amplitude-sensing system (fig. 16) two beams are formed with the axis symmetrically displaced from the desired boresight by a squint angle θ_s. The phase centers of each lobe are made to coincide and the amplitude patterns are mirror images of one another about the boresight. When using an array of transducers the pair of overlapping lobes may be produced in the beam former with a power splitter and two fixed delays for each element prior to summing, as shown in figure 16. Thus, the beam-steering delays are not affected by the use of

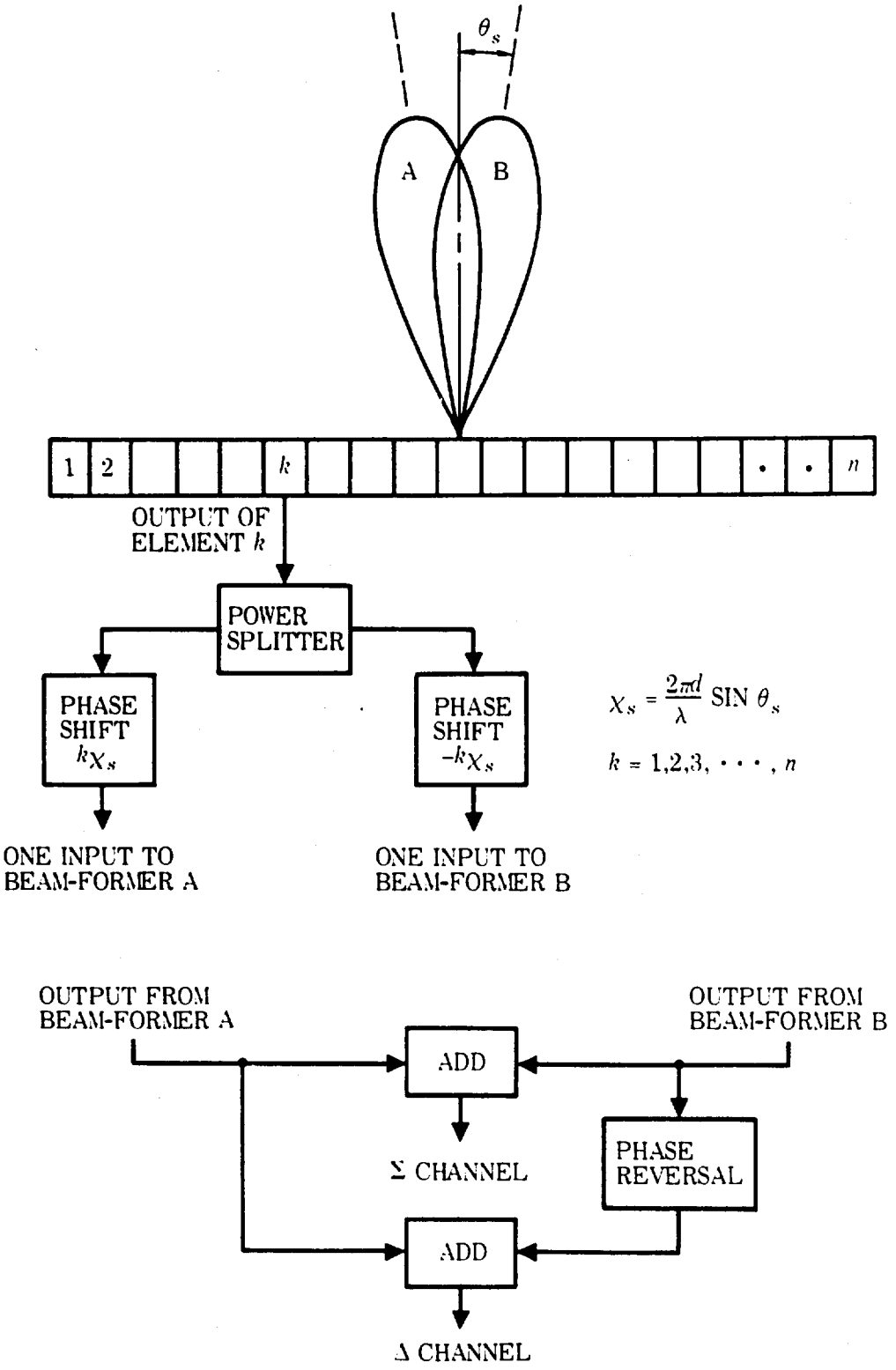

Figure 16. Amplitude-sensing monopulse.

monopulse tracking. For the case of uniform weighting of the elements, the outputs of the adjacent beams are given by

$$E_1 = D(p_1)\, A \cos \omega_0 t$$

$$E_2 = D(p_2)\, A \cos \omega_0 t$$

where

$$D(p_i) = \frac{\sin np_i}{n \sin p_i} \simeq \frac{\sin np_i}{np_i} \quad i = 1, 2$$

$$p_1 = \frac{\pi d}{\lambda}(\sin\theta - \sin\theta_s)$$

$$p_2 = \frac{\pi d}{\lambda}(\sin\theta - \sin\theta_s)$$

The sum and difference signals are

$$\Sigma = E_1 + E_2 = A[D(p_1) + D(p_2)] \cos \omega_0 t$$

$$\Delta = E_1 - E_2 = A[D(p_1) - D(p_2)] \cos \omega_0 t$$

The normalized difference signal is

$$\frac{\Delta}{\Sigma} = \frac{[D(p_1) - D(p_2)]}{[D(p_1) + D(p_2)]}$$

Figure 17 is a plot of the sum and difference patterns vs p for a cosine illuminated array. It is noted that one important parameter of the amplitude monopulse system is the squint angle, θ_s. The squint angle is usually chosen to give maximum linearity of the angle output, or for maximum sensitivity on the boresight, for a given illumination function. The Kerr-Murdock condition [11] shows that if the illumination function is a positive power of a half-cycle cosine, a squint angle of $np = \pi/2$ gives an output which is linear with angle off boresight. For the case where it is desired to maximize the boresight sensitivity the choice is not as simple. The sensitivity on boresight of the normalized difference signal is given by $\Delta(0)/\Sigma(0)$. Figures 18 and 19 show a plot of this function vs squint angle for uniformly illuminated and half-cycle cosine illuminated apertures. In both cases the sensitivity is a monotonically increasing function of squint angle and thus has no maximum within the sum beam width. In radar and sonar applications where the target is illuminated by the sum beam, there is logic in the selection of a squint angle which gives a maximum sum slope product. As is seen in the figures these maxima do exist and are found to be very close to the 3-dB power point independent

of the type of illumination function chosen. For uniform illumination the maximum is at $np = 1.30$ which is 2.6 dB down on the sum pattern. The 3-dB point is $np = 1.39$ and the 6-dB point is at 1.894. It was found that the sum slope product at the 6-dB point is about 0.8 of the sum slope product at the 3-dB point, or a loss of less than 1 dB.

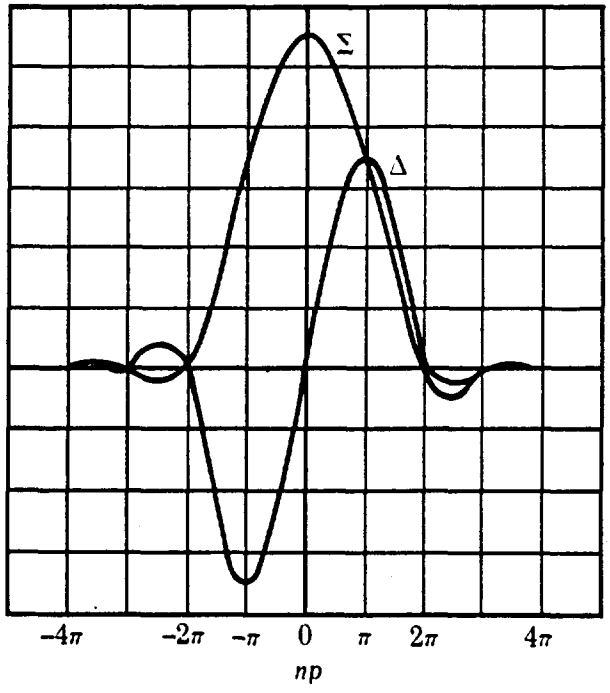

Figure 17. Sum and difference functions for a cosine-weighted additive array with $\theta_s = \theta_3$ dB.

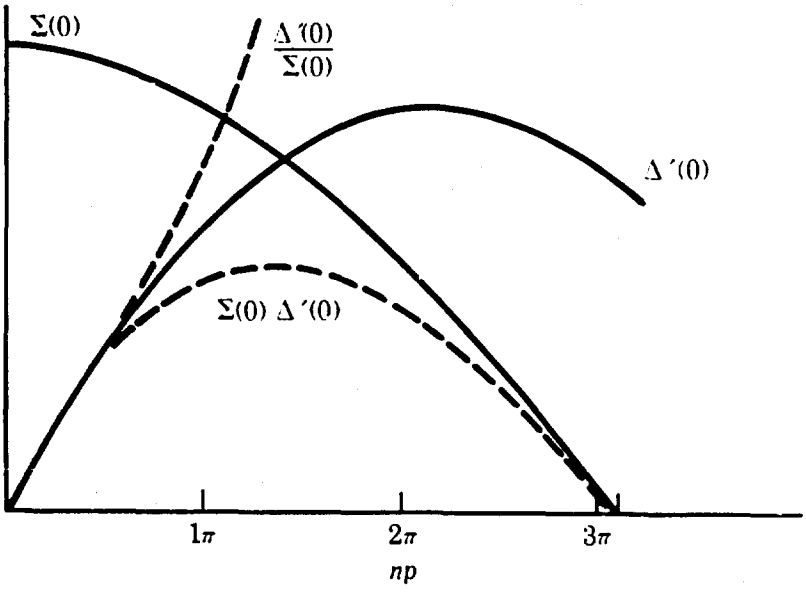

Figure 18. Functions of squint angle for uniform illumination.

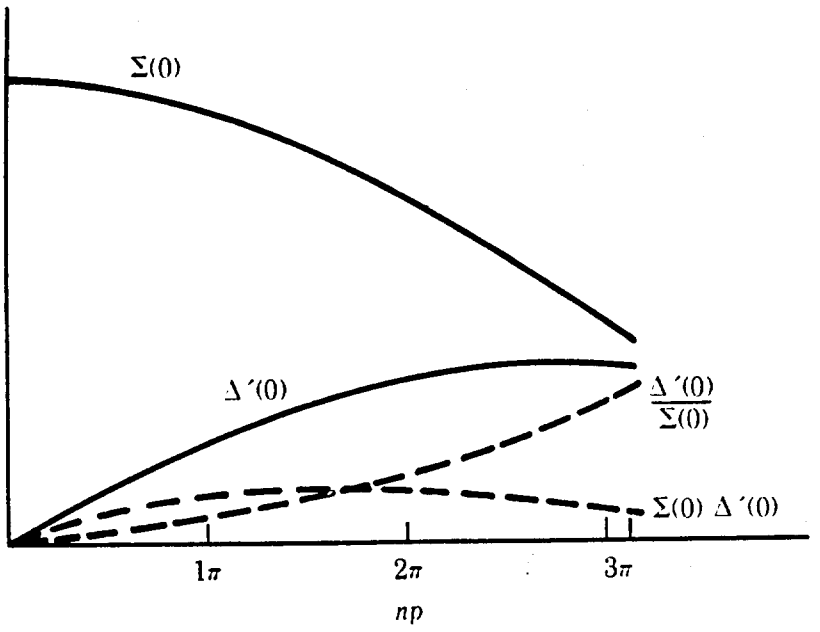

Figure 19. Functions of squint angle for cosine illumination.

Figure 20 is a block diagram of a processor for the sum and difference channels. Both channels are heterodyned to an i-f where they are amplified. The gain of the i-f amplifiers is controlled by the signal in the sum channel through the instantaneous automatic gain control (IAGC). Both channels are then applied to a phase comparator or phase-sensitivity amplitude detector which provides an output proportional to the difference over the sum and with the sign indicating sense.

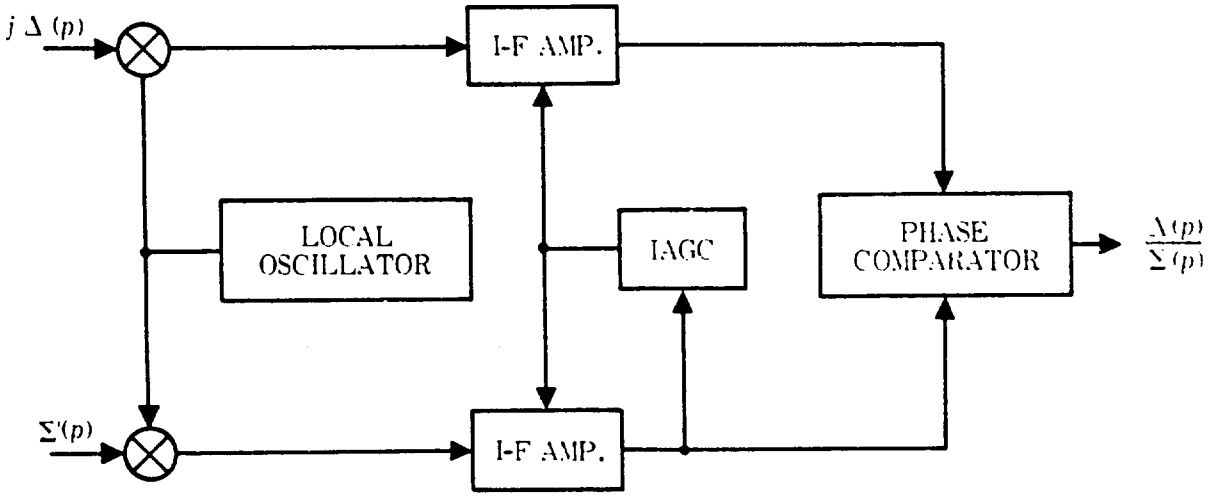

Figure 20. Example of monopulse processor for sum and difference channels.

The rms error in the estimate of angle of arrival using the monopulse will be many times less than the beam width of the sum channel for large signal-to-noise ratios. An estimate of that error is given by

$$\sigma_\theta = \frac{\theta_0}{K\left(\frac{2S}{N}\right)^{1/2}}$$

where

θ_0 is the half-power beam width

$\frac{S}{N}$ is the i-f signal-to-noise power ratio

K is the slope of the normalized difference signal in rms volts per beam width.

For the amplitude monopulse system with the squint angle equal to the 3-dB beam width, the slope is approximately 1.5 with uniform weighting. Thus, the normalized rms angular variance is

$$\left(\frac{\sigma\theta}{\theta_0}\right)^2 = \frac{N}{2K^2S} \simeq 0.222\left(\frac{N}{S}\right)$$

The phase-sensing monopulse system also forms sum and difference signals which may be processed in the same manner as for the amplitude-sensing system previously described. The difference is in the way the sum and difference signals are obtained. Figure 15 shows an additive array which forms a sum and difference signal by splitting the array into two sub-arrays. Since the arrays are the same size and both have parallel boresights, the far-field amplitude patterns will differ very little and only the phase of the sub-array outputs will differ, with the phase being a function of the angle of arrival. The amplitude of the i-f signal in the sum and difference channels was shown to be

$$|\Sigma| = An\,\frac{\sin np}{np}$$

$$|\Delta| = An\,\frac{\left(\sin\frac{np}{2}\right)^2}{\frac{hp}{2}}$$

For a fixed-length array, greater displacement of phase centers can be achieved by using only part of the array located near the extremes with an associated

increase in sensitivity to angle of arrival. However the maximum amplitude of the sum channel will be reduced in proportion to the percent of the array not used, and Rhodes [11] has shown that the maximum sum slope product is achieved when the full array is used with a phase center separation equal to half the array length. The normalized slope, k, used in estimating the rms angular error for the phase-sensing monopulse is approximately 1.4 for uniform weighting of the elements. Thus the normalized variance is

$$\left(\frac{\sigma_\theta}{\theta_0}\right)^2 = 0.255\left(\frac{N}{S}\right)$$

Some comments on the effects of phase and amplitude errors in the two types of systems may be helpful. In the amplitude-sensing system, any voltage unbalance prior to forming the sum and difference signals will cause a shift in the boresight; in the phase system any phase shift prior to forming sum and difference will cause a boresight shift. A shift in phase with the amplitude-sensing system will reduce the null depth, while with the phase-sensing system any voltage unbalance will cause a reduction in null depth. Phase shifts and voltage unbalances after the formation of the sum and difference signals will not affect the position or null depth, but will influence the sensitivity of the detector.[9]

Multiplicative Arrays

Multiplicative or cross-correlation receivers have been used to great advantage in many fields as a means of reducing the effective beam width of a system and thereby improving the angular resolution (ability to distinguish two adjacent targets). Most of these applications have involved (1) very long integration times, where the signal-to-noise ratio may be made as large as desired, and (2) passive detection techniques. The performance of the multiplicative array will be compared here with that of an additive array, for application to an active sonar or radar system.

In general, a line array of n elements may be combined in many ways by using only multiplication and averaging. Many interesting and unique directional patterns may be synthesized by this method, but all have the major disadvantage of having an output signal-to-noise ratio which is generally poorer than that of the smallest sub-array used. In addition, the response to multiple targets cannot in general be related to the position and relative amplitude of each target, because of the cross terms which arise in the multiplication. Reference 12 has a discussion for the response for two targets when a single multiplication is used. If only a single multiplication is allowed, an array of n elements may be divided into two sub-arrays of n_1 and n_2 elements. Each sub-array is operated as an additive line

array, and the outputs are then multiplied and averaged to produce a term at DC which is proportional to the input signal (fig. 21).

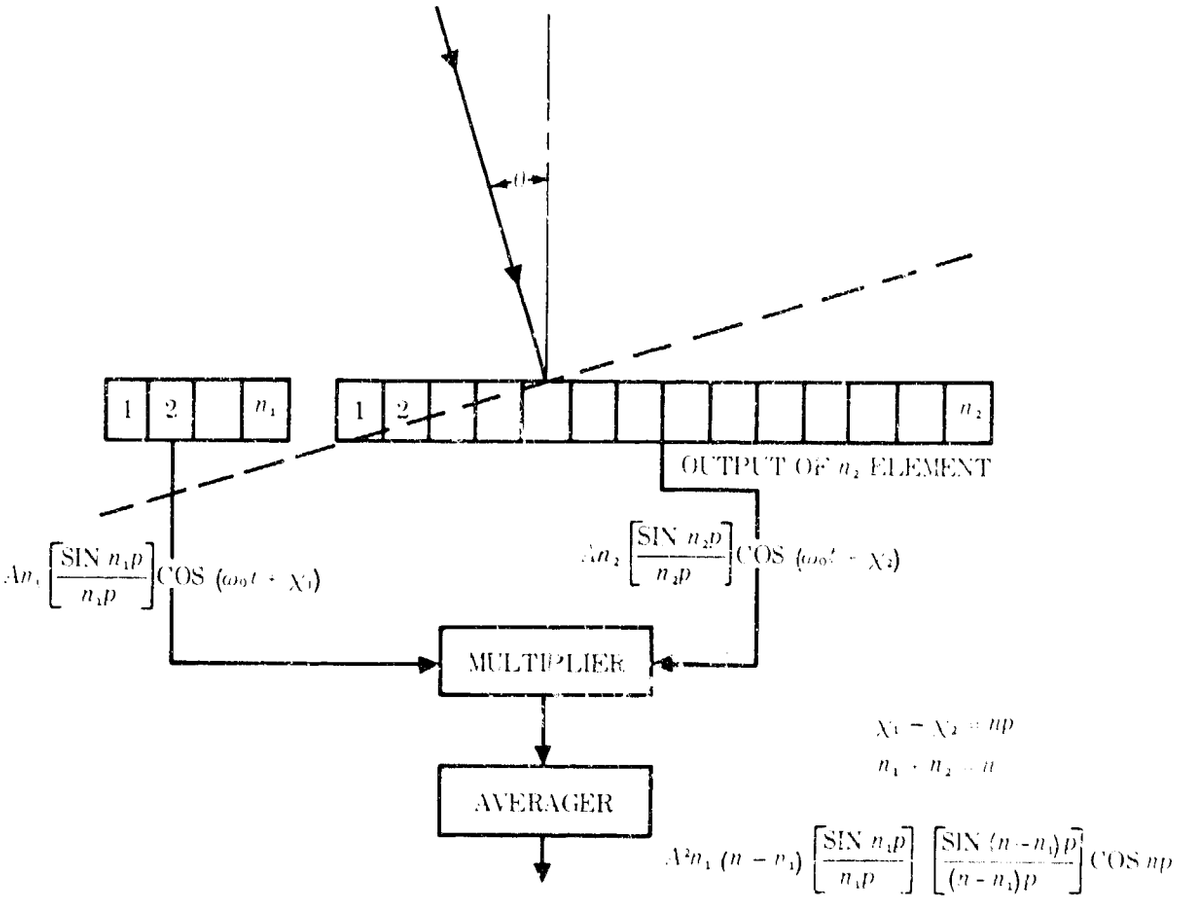

Figure 21. Multiplicative line array.

The directional function of each of the additive sub-arrays is given by

$$D_i(p) = \frac{\sin n_i p}{n_i \sin p} \quad i = 1, 2$$

where $p = \frac{\pi d}{\lambda} \sin \theta$ and d is the distance between equally spaced elements.* The result of multiplying two signals, $A \cos(\omega_0 t + \chi_1)$ and $B \cos(\omega_0 t + \chi_2)$, and supressing the term at $2\omega_0$ is

$$\frac{AB}{2} \cos(\chi_1 - \chi_2)$$

The phase difference between the outputs of each array is a function of the distance between phase centers, s, and the angle of arrival of the plane wave relative to broadside (no steering delays applied). Thus

$$\chi_1 = \frac{n_2}{2} \cdot \frac{2\pi d}{\lambda} \sin\theta$$

$$\chi_2 = -\frac{n_1}{2} \cdot \frac{2\pi d}{\lambda} \sin\theta$$

$$\chi_1 - \chi_2 = \frac{n_2 + n_1}{2}\left(\frac{2\pi d}{\lambda} \sin\theta\right) = np$$

The output after multiplying and averaging as a function of p is proportional to

$$D_m(p) = \left(\frac{\sin n_1 p}{n_1 \sin p}\right)\left(\frac{\sin n_2 p}{n_2 \sin p}\right)\cos np$$

or since $n_1 \cdot n_2 = n$ and $\sin p \simeq p$ for small element spacing

$$D_m(p) = \left(\frac{\sin n_1 p}{n_1 p}\right)\left(\frac{\sin (n - n_1) p}{(n - n_1) p}\right)\cos np$$

Note that the location of the first null is determined by the cos np term which is not a function of n_1 or n_2. The selection of n_1 and n_2 does affect the shape and side-lobe levels of the directional pattern as well as the signal-to-noise performance. (Reference 12 discusses the effect on side-lobe level.) The directional pattern of an additive array of n elements was shown to be proportional to

$$D_a(p) = \frac{\sin np}{np}$$

Note that the first null for the additive array occurs at $np = \pi$ while the first null for the multiplicative array is located at $np = \pi/2$. Thus the angular beam width to the first null of the multiplicative array is half that of the additive array of the same length.

In considering the effect of uncorrelated background noise on the reception of a single coherent signal, Welsby and Tucker [13] have shown that the rms signal-to-noise ratio, R (defined as the ratio of the dc terms to the ac terms out of the multiplier), is given by

$$R = \frac{R_1 R_2}{[\frac{1}{2}(1 + R_1^2 + R_2^2)]^{\frac{1}{2}}}$$

where R_1 and R_2 are the rms signal-to-noise ratios at the two inputs to the multiplier. If R_0 denotes the rms signal-to-noise ratio at each element and all elements have equal weighting, then $R_1 = \sqrt{n_1}\, R_0$ and $R_2 = \sqrt{n_2}\, R_0$ and

$$R = \frac{\sqrt{n_1 n_2}\, R_0^2}{[\frac{1}{2}(1 + n_1 R_0^2 + n_2 R_0^2)]^{\frac{1}{2}}}$$

If R_1 and R_2 are large compared to 1, then

$$R \sim R_0 \left(\frac{2n_1 n_2}{n_1 + n_2}\right)^{\frac{1}{2}}$$

or since $n_1 + n_2 = n$

$$R = R_0\sqrt{n}\, \left(\frac{2}{\frac{n}{n_2} + \frac{n}{n_1}}\right)^{\frac{1}{2}}$$

But $\sqrt{n}\, R_0$ is just the signal-to-noise ratio for an additive array of n elements; thus, the noise figure of the multiplicative array is given by

$$NF = \frac{(S/N)_a}{(S/N)_m} = \left[\frac{1}{2}\left(\frac{n}{n_1} + \frac{n}{n_2}\right)\right]^{\frac{1}{2}}$$

$$= \left[1 + \frac{1}{2}\left(\frac{n_2}{n_1} + \frac{n_1}{n_2}\right)\right]^{\frac{1}{2}}$$

Figure 22 is a plot of the noise figure as a function of the ratio of n_1 n_2 assuming $R_1^2 + R_2^2 \gg 1$. The minimum noise figure is equal to $\sqrt{2}$ when n_1 n_2 1. Thus, the multiplicative array has a signal-to-noise degradation of at least 3 dB compared to an additive array of equal length. As the ratio of n_1 n_2 becomes large the noise figure approaches $(n\ 2)^{\frac{1}{2}}$. Thus when n_2 1 the noise figure becomes progressively worse as the number of elements is increased. This is because the signal-plus-noise for the single element is always one of the inputs to the multiplier and output signal-to-noise ratio cannot be greater than that of the single element.

Setting n_1 n_2 $n\ 2$ to maximize the signal-to-noise ratio, the output of each sub-array due to a signal $A \cos \omega_0 t$ insistent at an angle θ (fig. 23) is given by

$$E_1 \quad \frac{An}{2} \left(\frac{\sin \frac{np}{2}}{\frac{np}{2}}\right) \cos (\omega_0 t + \chi)$$

$$E_2 = \frac{An}{2}\left(\frac{\sin\frac{np}{2}}{\frac{np}{2}}\right)\cos(\omega_0 t - \chi)$$

$$\chi = \frac{n}{4}\frac{2\pi d}{\lambda}\sin\theta = \frac{np}{2}$$

$$\Sigma = E_1 E_2 = \left(\frac{An}{2}\right)^2\left(\frac{\sin\frac{np}{2}}{\frac{np}{2}}\right)^2 [\cos(\omega_0 t + \chi)\cdot\cos(\omega_0 t - \chi)]$$

$$= \left(\frac{An}{2}\right)^2\left(\frac{\sin\frac{np}{2}}{\frac{np}{2}}\right)^2\left(\frac{1}{2}\cos 2\chi\right)$$

(neglecting the $2\omega_0 t$ term)

$$\Sigma = E_1 E_2 = \frac{(An)^2}{8}\left(\frac{\sin\frac{np}{2}}{\frac{np}{2}}\right)^2 \cos np$$

$$NF = \left[1 + 1/2\left(\frac{n_1}{n_2} + \frac{n_2}{n_1}\right)\right]^{1/2}$$

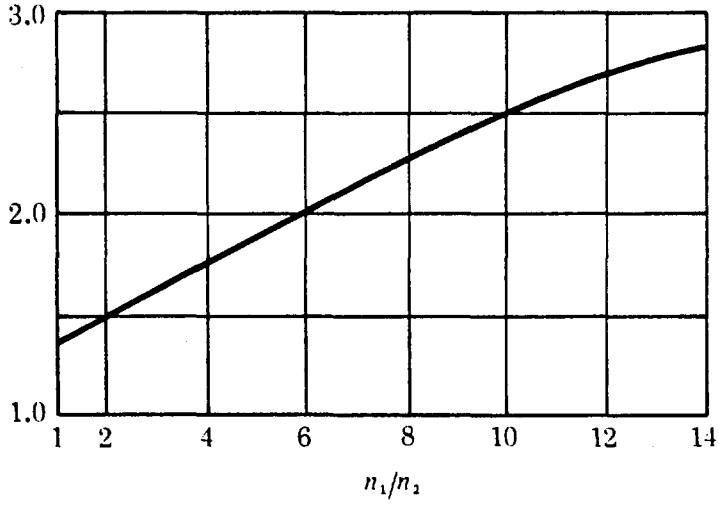

Figure 22. Noise figure of multiplicative array as a function of the ratio n_1/n_2.

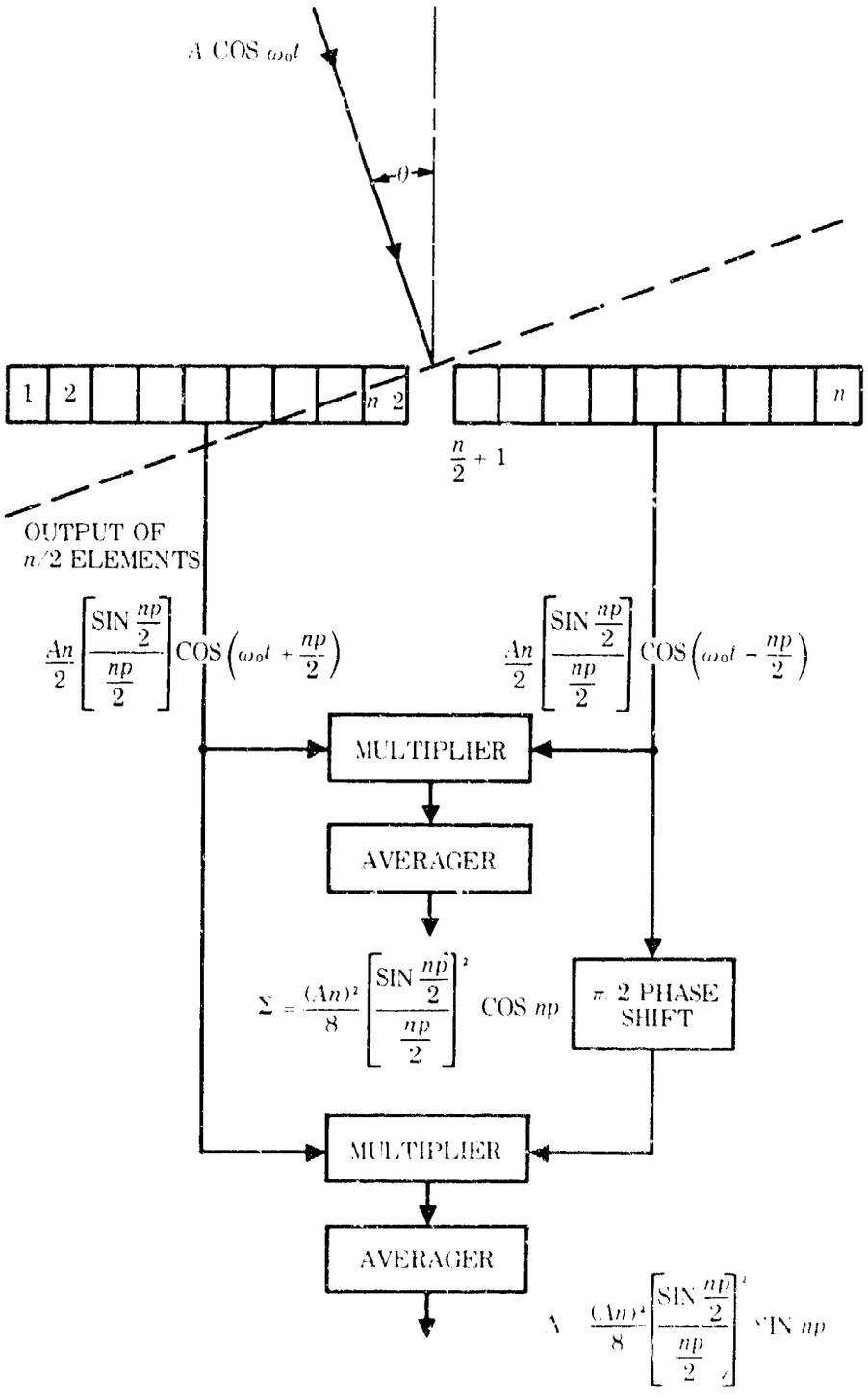

Figure 23. Split-beam multiplicative line array.

Figure 24 is a plot of the array response vs the parameter p for the split-beam multiplicative array with $n_1/n_2 = 1$ and $n_1/n_2 = 8$ compared with that of a uniform additive array.

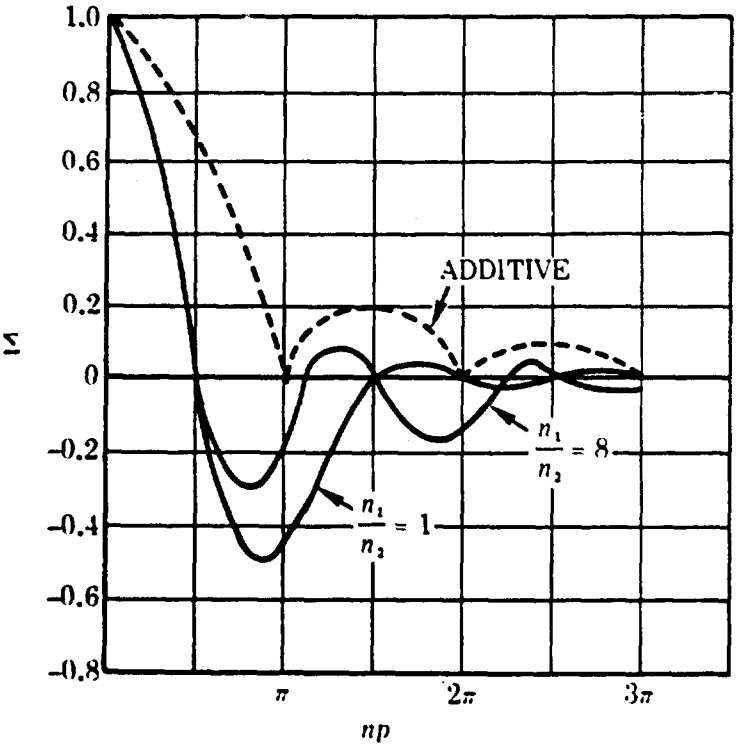

Figure 24. Σ pattern for multiplicative arrays.

For bearing determination using a split-beam multiplicative system, a phase shift of π 2 radians is introduced in one channel before multiplication to provide a signal which is an odd function of angle of arrival and has a null at boresight:

$$E_1 = \frac{An}{2}\left(\frac{\sin\frac{np}{2}}{\frac{np}{2}}\right)\cos(\omega_0 t - \chi)$$

$$E_2 = \frac{An}{2}\left(\frac{\sin\frac{np}{2}}{\frac{np}{2}}\right)\sin(\omega_0 t - \chi)$$

$$\Lambda = E_1 E_2 = \left(\frac{An}{2}\right)^2\left(\frac{\sin\frac{np}{2}}{\frac{np}{2}}\right)^2[\cos(\omega_0 t - \chi)\sin(\omega_0 t - \chi)]$$

$$\Delta = \left(\frac{An}{8}\right)^2 \left(\frac{\sin\frac{np}{2}}{\frac{np}{2}}\right)^2 \sin np$$

This function is plotted in figure 25 with $An \equiv 1$. The slope of this function at boresight ($p \equiv 0$) is twice that of the split-beam additive array null function. Since the signal-to-noise voltage ratio is down by the $\sqrt{2}$, the multiplicative split-beam system is the $\sqrt{2}$ more sensitive to arrival angle near the boresight when using normalized sum-and-difference systems.

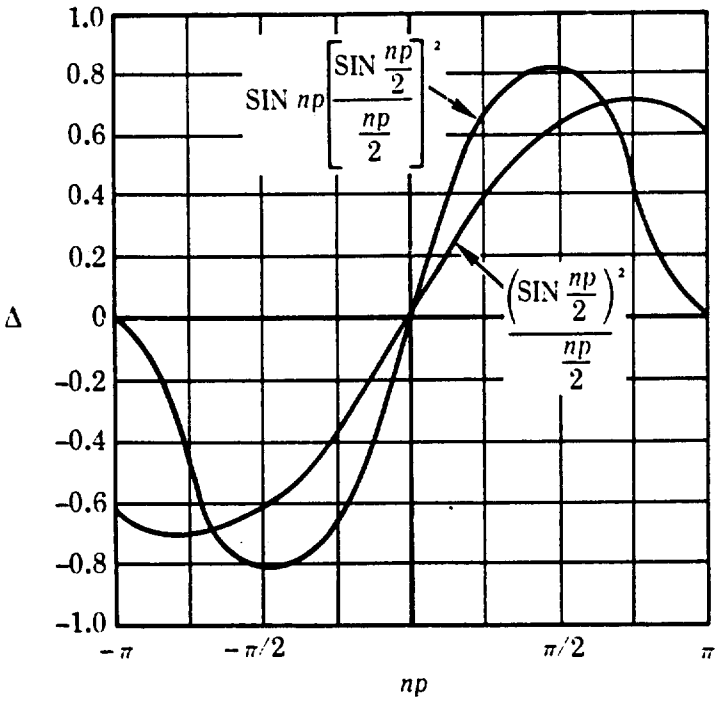

Figure 25. Δ pattern for split-beam multiplicative array.

Interferometers

For the purpose of completeness, the characteristics of the two-element additive and multiplicative interferometers will be given. Figures 26 and 27 show a two-element interferometer separated by a distance $D = nd$. The output of each element as a function of the angle of arrival is given by

$$E_1 = A \frac{\sin p}{p} \cos(\omega_0 t + \chi)$$

$$E_2 = A \frac{\sin p}{p} \cos (\omega_0 t - \chi)$$

$$p = \frac{\pi d}{\lambda} \sin \theta$$

$$\chi = np$$

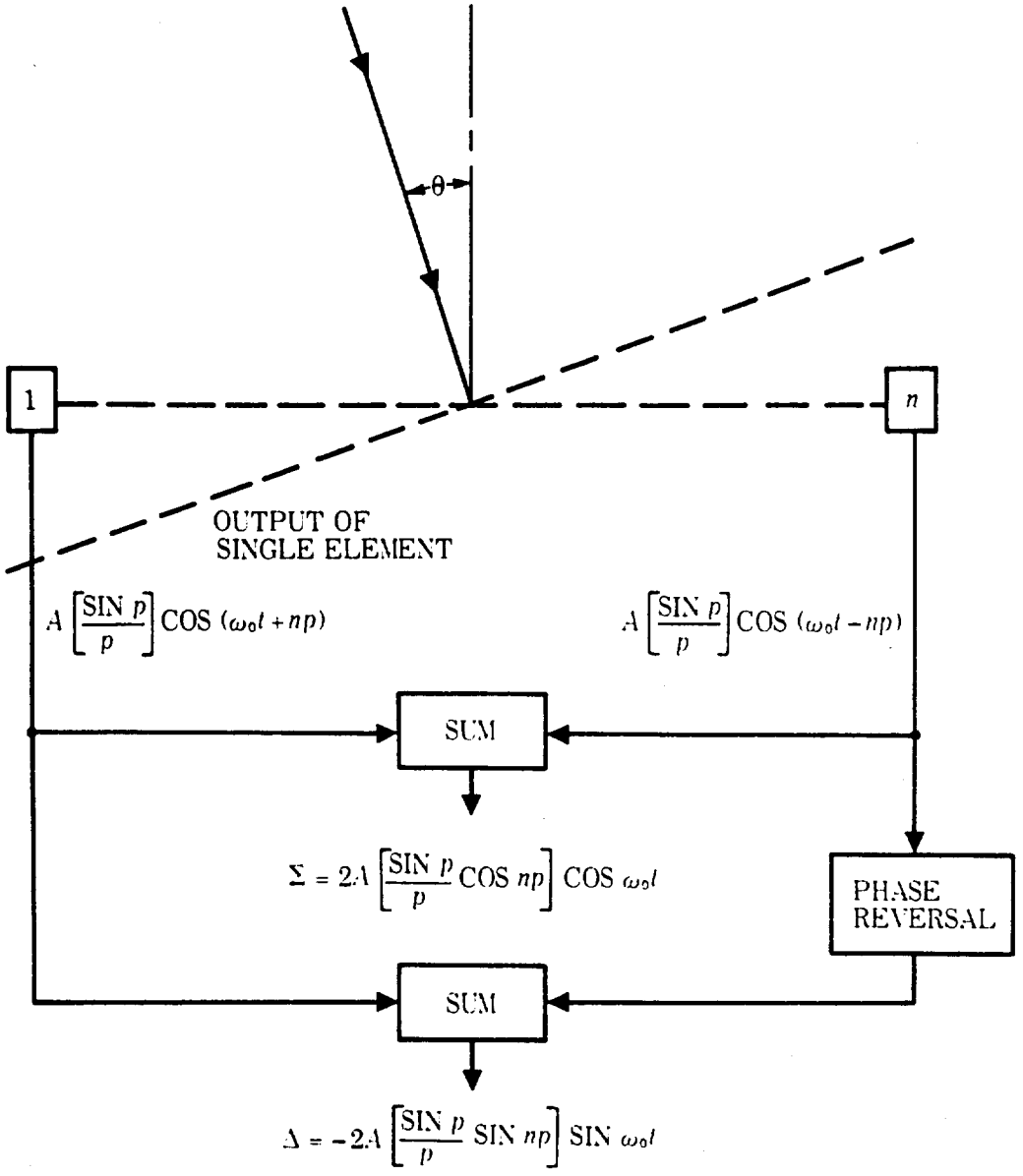

Figure 26. Additive interferometer.

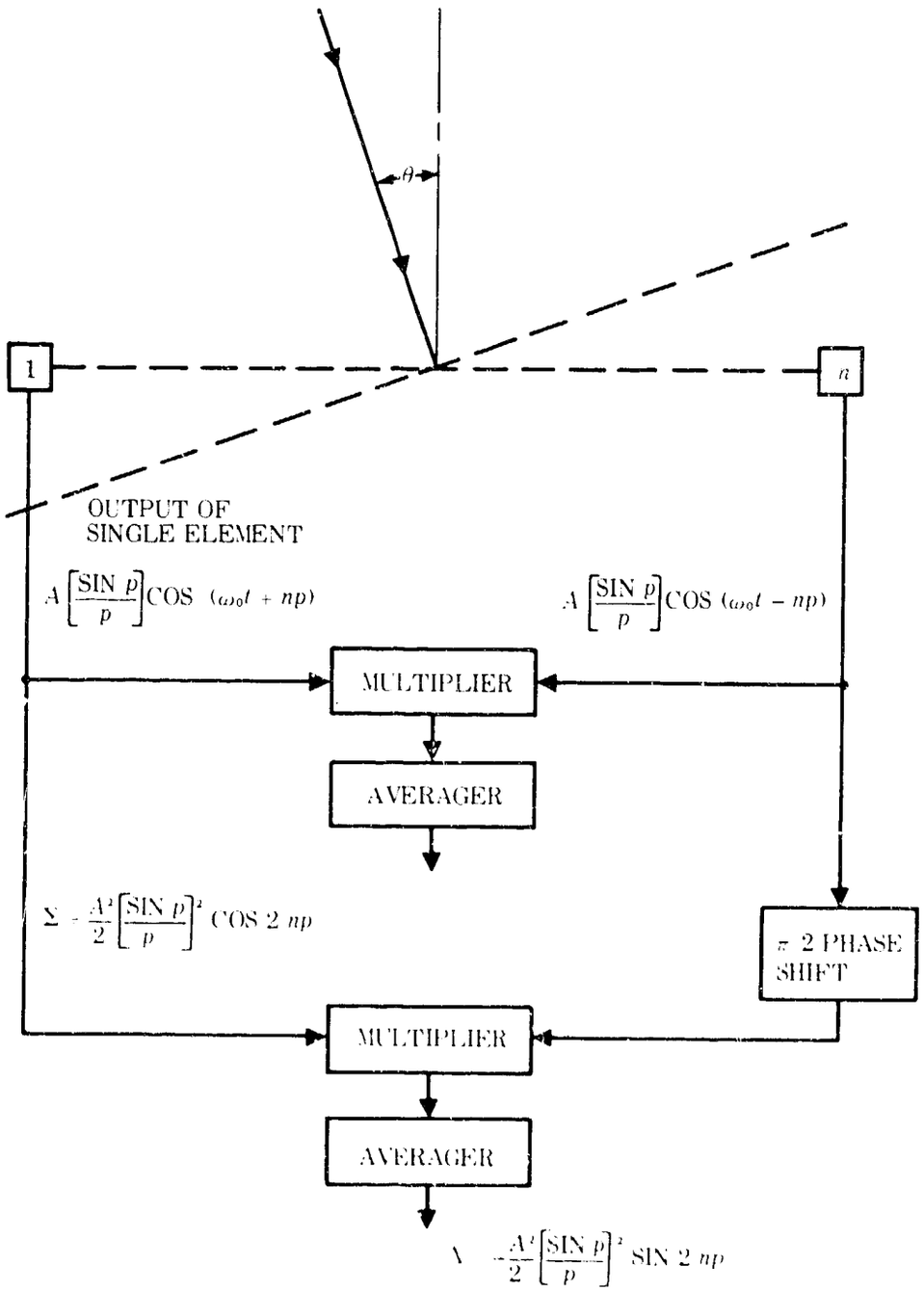

Figure 27. Multiplicative interferometer.

For the additive interferometer (fig. 26) the sum channel output is given by

$$\Sigma = E_1 + E_2 = A\left(\frac{\sin p}{p}\right)[2(\cos \omega_0 t)(\cos \chi)]$$

$$\Sigma = 2A\left(\frac{\sin p}{p} \cos np\right) \cos \omega_0 t$$

and the difference channel by

$$\Delta = 2A\left(\frac{\sin p}{p}\right)[2(\sin \omega_0 t)(\sin -\chi)]$$

$$\Delta = -2A\left(\frac{\sin p}{p} \cdot \sin np\right) \sin \omega_0 t$$

Thus the additive interferometer has a main beam width half that of a full additive array whose length is equal to the interferometer spacing. This is because the phase centers are approximately twice as far apart. However, the signal-to-noise performance is down by $\sqrt{n/2}$ because of the use of fewer elements, and grating lobes of almost equal gain as the main lobe will appear at $np = k\pi$, $k = 1, 2, 3, \cdots$ giving angular ambiguities.

For the multiplicative interferometer the beam-forming channel output (fig. 27) will be

$$\Sigma = E_1 E_2 = A^2\left(\frac{\sin p}{p}\right)^2 (\tfrac{1}{2} \cos 2\chi)$$

$$= \frac{A^2}{2}\left(\frac{\sin p}{p}\right)^2 \cos 2\, np$$

The null channel will give

$$\Delta = A^2\left(\frac{\sin p}{p}\right)^2 \left(\frac{1}{2} \sin -2\chi\right)$$

$$= -\frac{A^2}{2}\left(\frac{\sin p}{p}\right)^2 \sin 2\, np$$

Thus the multiplicative interferometer reduces beam width by a factor of 2 and gives twice as many grating lobes as the additive interferometer. The power signal-to-noise ratio for the multiplicative system is reduced by 3 dB over the additive system, as expected.

Comparison of Systems

A summary of the characteristics of the various systems is contained in tables 2 and 3. Table 2 gives the directional patterns for the beam-forming systems where the amplitude of the additive array has been normalized to 1 at the peak response and all other systems are referenced to the additive system. The location of the first null is used as an indication of the main lobe width and the noise factor is defined as the ratio of the signal-to-noise for the additive system over that of the system considered. Thus an increase in the noise factor represents a poorer signal-to-noise performance for a coherent signal and for uniformly distributed, uncorrelated noise.

TABLE 2. CHARACTERISTICS OF BEAM-FORMING SYSTEM

Technique	Directional Pattern	Location of 1st Null	Noise Factor (ratio)	Noise Factor (dB)
Uniformly illuminated additive array	$\frac{\sin np}{np}$	$p = \frac{\pi}{n}$	1 (ref.)	0
Cosine taper additive array $2\cos\frac{k\pi}{n}$ $k = 0, \pm 1, \pm 2, \cdots \pm n/2$	$\frac{\sin\left(np-\frac{\pi}{2}\right)}{\left(np-\frac{\pi}{2}\right)} + \frac{\sin\left(np+\frac{\pi}{2}\right)}{\left(np+\frac{\pi}{2}\right)}$	$p = \frac{3\pi}{2n}$	1.11	0.92
Split-beam multiplicative array	$\frac{1}{8}\left(\frac{\sin\frac{np}{2}}{\frac{np}{2}}\right)^2 \cos np$	$p = \frac{\pi}{2n}$	$\frac{\sqrt{2}}{S/N} \cdot 1$	3.0
Additive interferometer	$\frac{2}{n}\frac{\sin p}{p}\cos np$	$p = \frac{\pi}{2n}$	$\sqrt{n/2}$	--
Multiplicative interferometer	$\frac{1}{2n^2}\left(\frac{\sin p}{p}\right)^2 \cos 2np$	$p = \frac{\pi}{4n}$	$\frac{\sqrt{n}}{S/N} \cdot 1$	--

Table 3 compares the same systems when used for estimating bearing with a null pattern. Again the additive array is taken as a reference with its amplitude normalized. The measure of performance for a nulling system is the slope at the null, normalized by the peak value of the signal, times the signal-to-noise ratio. The slope at the null is a function of the peak signal value unless the null channel is normalized by the beam forming channel such as is done with a true

monopulse system. The S/N ratio is important in locating the null since the noise in the null channel is the factor which produces an error in estimating the angle. A comparative ratio similar to that defining the noise figure is given by

$$\Gamma = \frac{\left[\left(\frac{d\Lambda}{d\theta}\right)_{\theta=0}\left(\frac{1}{\Sigma}\right)_{\theta=0}\left(\frac{S}{N}\right)\right]_{\text{additive}}}{\left[\left(\frac{d\Lambda}{d\theta}\right)_{\theta=0}\left(\frac{1}{\Sigma}\right)_{\theta=0}\left(\frac{S}{N}\right)\right]_{\text{system}}}$$

where Λ is the null channel directional pattern and Σ is the beam-forming channel directional pattern. The numerator is related to the additive array which is used

TABLE 3. CHARACTERISTICS OF NULL SYSTEM

System		β (rate)	Γ (ratio)	Γ (dB)
Uniformly illuminated difference system	$\frac{\left(\sin\frac{np}{2}\right)^2}{\frac{np}{2}}$	1	1	0
Sine taper $2\sin\left(\frac{k\pi}{n}\right)$ $k = 0, \pm 1, \pm 2, \cdots \pm n/2$	$\frac{\sin\left(np-\frac{\pi}{2}\right)}{np-\pi/2} - \frac{\sin\left(np-\frac{\pi}{2}\right)}{np+\pi/2}$	$\frac{\pi}{4}$	0.87	-1.2
Split-beam multiplicative array	$\frac{1}{8}\left(\frac{\sin\frac{np}{2}}{\frac{np}{2}}\right)^2 \sin np$	$\frac{1}{2}$	$\frac{1}{\sqrt{2}}$ $S/N = 1$	-3.0
Additive interferometer	$\frac{2}{n}\frac{\sin p}{p}\sin np$	$\frac{1}{2}$	$\frac{1}{2}\sqrt{n/2}$	--
Multiplicative interferometer	$\frac{1}{2n^2}\left(\frac{\sin p}{p}\right)^2 \sin 2np$	$\frac{1}{4}$	$\frac{1}{4}\sqrt{n}$ $S/N = 1$	--

for reference and the denominator is related to the system being compared. Table 3 also gives the ratio of the normalized slopes of

$$\beta = \frac{\left[\left(\frac{\partial \Lambda}{\partial \theta}\,\frac{1}{\Sigma}\right)_{\theta=0}\right]_{\text{additive}}}{\left[\left(\frac{\partial \Lambda}{\partial \theta}\,\frac{1}{\Sigma}\right)_{\theta=0}\right]_{\text{system}}}$$

therefore

$$\Gamma = \beta \frac{\left(\frac{S}{V}\right)_{\text{additive}}}{\left(\frac{S}{V}\right)_{\text{system}}}$$

SUMMARY AND CONCLUSIONS

A comparison of the techniques for processing the information from a line array of elements has shown that it is possible to obtain improvement in one system characteristic (i.e., angular resolution) at the expense of another (i.e., signal-to-noise). The criterion for selecting any particular technique is the importance of each system parameter to overall system performance. If, as is often the case, the maximization of signal-to-noise ratio is most important, it was shown that a uniformly illuminated additive array provides the best signal-to-noise ratio for a given array size and for uncorrelated uniformly distributed noise background. Any reduction in signal-to-noise ratio will result in a reduced probability of detection. Thus, for detection in a noise background, the additive array is best. If, on the other hand, some sacrifice in detection probability can be tolerated in exchange for improved angular resolution, a split-beam multiplicative system provides a main-lobe beam width half as wide as that of an additive array of the same length with a loss of 3 dB in signal-to-noise power ratio.

The use of only the two end elements of the array in an additive interferometer provides the same angular resolution that is possible with the split-beam multiplicative array, but at a great loss in signal-to-noise and with the addition of ambiguities in angle due to the grating lobes. The use of the same two end elements in a multiplicative interferometer provides improvement in angular resolution (by a factor of 2) over the additive interferometer, in exchange for a 3-dB loss in signal-to-noise ratio and a doubling of the number of grating lobes.

The multiplicative system produces cross terms which, in the case of multiple targets, may result in outputs that have no correlation with the target positions. To prevent these undesired outputs, range gating within each beam will be necessary to provide resolution in range.

To improve the accuracy of the estimate of bearing, a "nulling" system may be used with any of the beam-forming systems discussed. In general the nulling systems are the same as the beam-forming systems, except that in the additive systems a phase shift of π radians is introduced in one arm prior to summing and in the multiplicative systems a shift of $\pi/2$ radians is made prior to multiplying. In comparing the nulling systems, two parameters are important. The slope of the function near the null is related both to the sensitivity to displacements from the null and to the rms value of the noise present in the null channel for some standard input, since at the null the noise level produces the error in the angular estimate. In table 3 the directional patterns of the nulling systems associated with the beam-forming systems of table 2 are given. The ratio β is the slope of the directional function at the null normalized by the peak signal from the beam-forming function. These have been compared with the uniformly illuminated additive array again and the smaller the ratio the greater the slope. The function Γ is equal to β times the ratio of the signal-to-noise ratios (the noise factor

given in table 2). Table 3 shows that the sine taper provides slightly (~1.2 dB) better angular accuracy despite the slightly (0.92 dB) poor signal-to-noise performance. The split-beam multiplicative array provides a factor of $\sqrt{2}$ improvement in angular accuracy and a factor of 2 improvement in angular resolution, in exchange for the 3-dB loss in signal-to-noise ratio. All the nulling systems assume that only a single target is present within a resolution cell.

It appears that the small improvement in angular accuracy and resolution available with the split-beam multiplicative systems are not worth the price of a 3-dB loss in signal-to-noise in an ASW situation where detection is of prime importance.

REFERENCES

1. Barton, D.K., Radar System Analysis, Prentice-Hall, 1964

2. Berman, A. and Clay, C.S., "Theory of Time-Averaged-Product Arrays," Acoustical Society of America. Journal, v.29, p.805-812, July 1957

3. Blommendaal, R., "A Note on Multiplicative Receiving Systems for Radar," Radio and Electronic Engineer, v.28, p.317-324, November 1964

4. Brown, J.L., Jr. and Towlands, R.O., "Design of Directional Arrays," Acoustical Society of America. Journal, v.31, p.1638-1643, December 1959

5. Cohen, W. and Steinmetz, C.M., "Amplitude-and Phase-Sensing Monopulse System Parameters, Part I," Microwave Journal, v.2, p.27-33, October 1959

5a. Cohen, W. and Steinmetz, C.M., "Amplitude-and Phase-Sensing Monopulse System Parameters, Part II," Microwave Journal, v.2, p.33-38, November 1959

6. Dolph, C.L., "A Current Distribution for Broadside Arrays Which Optimizes the Relationship Between Beam Width and Side Lobe Level," Institute of Radio Engineers. Proceedings, v.34, p.335-348, June 1946

7. Hansen, R.C., "Gain Limitations of Large Antennas," Institute of Radio Engineers. Transactions: Antennas and Propagation, v.AP-8, p.490-495, September 1960

8. Hansen, R.C., "Tables of Taylor Distributions for Circular Aperture Antennas," Institute of Radio Engineers Transactions: Antennas and Propagation, v.AP-8, p.23-26, January 1960

9. Jacobson, M.J., "Analysis of a Multiple Receiver Correlation System," Acoustical Society of America. Journal, v.29, p.1342-1347, December 1957

10. Kraus, J.D., Antennas, Chapter 4, McGraw-Hill, 1950

11. Ksienski, A., "Multiplicative Processing Antenna Systems for Radar Applications," Radio and Electronic Engineer, v.29, p.53-67, January 1965

12. Ksienski, A., "Signal Processing Antenna (1)," Microwave Journal, v.4, p.77-85, October 1961

12a. Ksienski, A., "Signal Processing Antenna (2)," Microwave Journal, v.4, p.87-94, November 1961

13. Manasse, R., "Maximum Angular Accuracy of Tracking a Radio Star by Lobe Comparison," Institute of Radio Engineers. Transactions: Antennas and Propagation, v.AP-8, p.50-56, January 1960

14. McCartney, B.S., "Theoretical and Experimental Properties of Two-Element, Multiplicative Multi-Frequency Receiving Arrays Including Superdirectivity," Radio and Electronic Engineer, v.28, p.129-144, August 1964

15. Canada. RCA Victor Company, Ltd. Report 6.501.3, A Survey of Array Theory and Techniques, by H.J. Moody, November 1963 (AD 430028)

16. Polk, C., "Transient Behavior of Aperture Antennas," Institute of Radio Engineers. Proceedings, v.48, p.1281-1288, July 1960

17. Price, O.R. and Hyneman, R.F., "Distribution Functions for Monopulse Antenna Difference Patterns," Institute of Radio Engineers. Transactions: Antennas and Propagation, v.AP-8, p.567-576, November 1960

18. Philco Scientific Laboratory Contract AF 19(628)-2403; Scientific Report 1, Advanced Antenna Techniques, by L.W. Procopio and others, October 1963

19. Rhodes, D.R., Introduction to Monopulse, McGraw-Hill, 1959

20. Schell, A.C., "Enhancing the Angular Resolution of Incoherent Sources," Radio and Electronic Engineer, v.29, p.21-26, January 1965

21. Shaw, E. and Davies, D.E.N., "Theoretical and Experimental Studies of the Resolution Performance of Multiplicative and Additive Aerial Arrays," Radio and Electronic Engineer, v.28, p.279-291, October 1964

22. Skolnik, M.I., Introduction to Radar Systems, McGraw-Hill, 1962

23. Stegen, R.J., "Excitation Coefficients and Beamwidths of Tschebycheff Arrays," Institute of Radio Engineers. Proceedings, v.41, p.1671-1674, November 1953

24. Taylor, T.T., "Design of Line-Source Antennas for Narrow Beamwidth and Low Side Lobes," Institute of Radio Engineers. Transactions: Antennas and Propagation, v.AP-3, p.16-28, January 1955

25. Thomas, J.B. and Williams, T.R., "On the Detection of Signals in Nonstationary Noise by Product Arrays," Acoustical Society of America. Journal, v.31, p.453-462, April 1959

26. Tucker, D.G., "The Signal-Noise Performance of Electro-Acoustic Strip Arrays," Acustica, v.8, p.53-62, 1958

27. Welsby, V.G. and Tucker, D.G., "Multiplicative Receiving Arrays," British Institution of Radio Engineers, London. Journal, v.19, p.369-382, June 1959

28. Van der Maas, G.J., "A Simplified Calculation for Dolph-Tchebycheff Arrays," Journal of Applied Physics, v.25, p.121-124, January 1954

29. Von Aulock, W.H., "Properties of Phased Arrays," Institute of Radio Engineers. Proceedings, v.48, p.1715-1727, October 1960

UNCLASSIFIED

Security Classification

DOCUMENT CONTROL DATA - R & D

(Security classification of title, body of abstract and indexing annotation must be entered when the overall report is classified.)

1. ORIGINATING ACTIVITY (Corporate author)

Navy Electronics Laboratory
San Diego, California 92152

2a. REPORT SECURITY CLASSIFICATION

UNCLASSIFIED

2b. GROUP

3. REPORT TITLE

RESPONSES OF ARRAYS OF ISOTROPIC ELEMENTS IN DETECTION AND TRACKING

4. DESCRIPTIVE NOTES (Type of report and inclusive dates)

Research Report July 1966 - February 1967

5. AUTHOR(S) (First name, middle initial, last name)

L. K. Arndt

6. REPORT DATE	7a. TOTAL NO. OF PAGES	7b. NO. OF REFS
21 April 1967	62	29

8a. CONTRACT OR GRANT NO.	9a. ORIGINATOR'S REPORT NUMBER(S)
b. PROJECT NO. S23-26 Task 8553	1456
c. (NEL J80173)	9b. OTHER REPORT NO(S) (Any other numbers that may be assigned this report)
d.	

10. DISTRIBUTION STATEMENT

11. SUPPLEMENTARY NOTES	12. SPONSORING MILITARY ACTIVITY
	Naval Ship Systems Command Department of the Navy

13. ABSTRACT

Analytical expressions of responses for linear, planar, cylindrical, and spherical arrays are given. Additive arrays are found "best" for detection of a point target in a uniform noise field. Split-beam multiplicative arrays are found "best" for bearing estimates of a single point target.

DD FORM 1 NOV 65 1473 (PAGE 1)

S/N 0101-807-6801

UNCLASSIFIED

Security Classification

14 KEY WORDS	LINK A		LINK B		LINK C	
	ROLE	WT	ROLE	WT	ROLE	WT
Arrays - Analysis						
Targets - Detection						

CHIEF OF NAVAL MATERIAL
MAT 03L
MAT 033
MAT 0331
PM4
COMMANDER, NAVAL SHIP SYSTEMS COMMAND
SHIPS 031
SHIPS 0343
SHIPS 0344
SHIPS 035
SHIPS 1610
SHIPS 1622
SHIPS 1622C
SHIPS 1623
SHIPS 1631
SHIPS 1632
SHIPS 1633
SHIPS 1634
SHIPS 2021 (2)
SHIPS 204113
COMMANDER, NAVAL AIR SYSTEMS COMMAND
AIR 5330
AIR 604
COMMANDER, NAVAL ORDNANCE SYSTEMS COMMAND
ORD 03C
ORD 0322
ORD 9132
COMMANDER, NAVAL ELECTRONIC SYSTEMS COMMAND
TECHNICAL LIBRARY
COMMANDER, NAVAL SHIP ENGINEERING CENTER
CODE 6170
CODE 6179B
CODE 6179C03
CODE 6360
CHIEF OF NAVAL PERSONNEL
PERS 11B
CHIEF OF NAVAL OPERATIONS
OP-03EG
OP-311
OP-312F
OP-322C
OP-345
OP-07C
OP-07T
OP-701
OP-702C
OP-71
OP-713
OP-715 (10)
OP-72
OP-724
OP-09B5
OP-09B5D
OP-912-B
OP-922Y4C1
OP-95
CHIEF OF NAVAL RESEARCH
CODE 408
CODE 416
CODE 418
CODE 455
CODE 466
CODE 468
COMMANDER IN CHIEF
US PACIFIC FLEET
CODE 93
US ATLANTIC FLEET
COMMANDER OPERATIONAL TEST & EVALUATION FORCE
DEPUTY COMMANDER OPERATIONAL TEST & EVALUATION FORCE, PACIFIC
COMMANDER CRUISER-DESTROYER FORCE
US PACIFIC FLEET
CODE 425
US ATLANTIC FLEET
COMMANDER SUBMARINE FORCE
US PACIFIC FLEET
US ATLANTIC FLEET
COMMANDER ANTISUBMARINE WARFARE FORCE
US PACIFIC FLEET
US ATLANTIC FLEET
COMMANDER FIRST FLEET
COMMANDER SUBMARINE DEVELOPMENT GROUP 2
COMMANDER DESTROYER DEVELOPMENT GROUP, PACIFIC
COMMANDER FLEET AIR WINGS,
US PACIFIC FLEET
US ATLANTIC FLEET
SCIENTIFIC ADVISORY TEAM
NAVAL AIR DEVELOPMENT CENTER
LIBRARY
NAVAL MISSILE CENTER
TECHNICAL LIBRARY
PACIFIC MISSILE RANGE
CODE 3250
CODE 624.3
NAVAL AIR TEST CENTER
WEAPONS SYSTEMS TEST DIVISION
NAVAL AIR MINE DEFENSE DEVELOPMENT UNIT
NAVAL RESEARCH & DEVELOPMENT CENTER
CARDEROCK DIVISION
LIBRARY
CODE 900
ANNAPOLIS DIVISION
NAVY UNDERWATER SOUND LABORATORY
LIBRARY
CODE 905
CODE 920
CODE 930
ATLANTIC FLEET ASW TACTICAL SCHOOL
LIBRARY
NAVAL RESEARCH LABORATORY
CODE 2027
CODE 5540
NAVAL ORDNANCE LABORATORY
WHITE OAK
DIVISION 221
DIVISION 730
DIVISION 880
NAVY UNDERWATER SOUND REFERENCE LABORATORY
LIBRARY
NAVAL UNDERWATER WEAPONS RESEARCH & ENGINEERING STATION
LIBRARY
OFFICE OF NAVAL RESEARCH BRANCH OFFICE
PASADENA
CHIEF SCIENTIST
NAVAL POSTGRADUATE SCHOOL
LIBRARY (2)
NAVAL APPLIED SCIENCE LABORATORY
CODE 9200
CODE 9832
NAVAL WAR COLLEGE
ARMED FORCES STAFF COLLEGE
ADMINISTRATIVE COMMAND
ASSISTANT SECRETARY OF THE NAVY (RESEARCH & DEVELOPMENT)
DOD RESEARCH & ENGINEERING
TECHNICAL LIBRARY
WEAPONS SYSTEMS EVALUATION GROUP
DEFENSE DOCUMENTATION CENTER (20)
ARMY RESEARCH & DEVELOPMENT ACTIVITY
ELECTRONIC WARFARE DIVISION
REDSTONE SCIENTIFIC INFORMATION CENTER
ARMY ELECTRONICS RESEARCH & DEVELOPMENT LABORATORY
ARMY ELECTRONICS COMMAND
MANAGEMENT & ADMINISTRATIVE SERVICES DEPT
AMSEL-RD-MAT
ELECTRONICS SYSTEMS DIVISION
ESTI
ROME AIR DEVELOPMENT CENTER
RCRES-4C